EVALUATING THE ENVELOPE PERFORMANCE OF COMMERCIAL OFFICE BUILDINGS IN CITIES

CHONG ZHUN MIN ADRIAN
(B.Sc.(Hons.), NUS)

A THESIS SUBMITTED

FOR THE DEGREE OF MASTER OF SCIENCE

(BUILDING)

DEPARTMENT OF BUILDING

NATIONAL UNIVERSITY OF SINGAPORE

2012

DECLARATION

I hereby declare that the thesis is my original work and has been written by me in its entirety. I have duly acknowledged all the sources of information which have been used in the thesis.

This thesis has also not been submitted for any degree in any university previously.

Chong Zhun Min Adrian
18 July 2012

Acknowledgments

Table of Contents

Executive summary

Over the past decade, the urban heat island (UHI) phenomenon and its corresponding issues and mitigation strategies have become a main research topic in the area of urban climatology and building science. In particular, Geographical Information System (GIS) has commonly been used as a platform to represent UHI prediction models and its influence on other issues such as natural ventilation and thermal comfort, thus allowing planning to proceed in a more informed manner. However, to date, there has been no study that has extended this representation to building performance at a macro scale level. To develop a sustainable city, it is not sufficient to only focus on urban canopy models and green building designs. An effective urban climate tool should integrate UHI prediction models with building performance, so that mitigation strategies can be evaluated effectively. This thesis shall present a methodology for evaluating the building performance of offices in cities while taking into account its surrounding morphology. The indices that are used to evaluate performance include solar radiation gains through glazing and conduction heat gains (through opaque walls, fenestration and roofs). This thesis also presents a method for morphing maximum, minimum and average temperatures (the output of air prediction model STEVE) into a typical 24 hour profile for use in building energy simulation programmes.

List of Tables

List of Figures

List of Symbols

α   = absorptance of surface

β   = solar altitude angle, °

δ   = solar declination, °

ε   = hemispherical emittance of surface

σ   = stefan boltzmann constant, W/m^2K^4

ρ   = ground reflectance

ϕ   = solar azimuth, °

Σ   = tilt angle, °

θ   = angle of incidence, °

Ψ   = surface azimuth, °

ω   = hour angle

A   = surface area, m²

AST   = apparent solar time, decimal hours

E   = radius of the earth, 6,356km

E_t = total solar radiation incident on surface, W/m²

E_b = beam/direct component of solar radiation incident on surface at hour t, W/m²

E_d = sky diffuse component of solar radiation incident on surface at hour t, W/m²

E_r = ground reflected component of solar radiation incident on surface at hour t, W/m²

ET   = equation of time, minutes

h_c = coefficient of heat transfer by convection, W/m²K

h   = coefficient of heat transfer by long-wave radiation and convection, W/m²K

h_r = coefficient of heat transfer by long-wave radiation, W/m²K

H_b = offset equal to zero for the troposphere, m

H_z = geopotential altitude, m

K   = conductivity, W/mK

K_d = ratio of diffuse radiation to global radiation

K_T = ratio of global radiation to extraterrestrial radiation

L = latitude, (°N, negative in southern hemisphere)

LST = local solar time, decimal hours

$LSTM$ = longitude of local standard time meridian, °E of Greenwich (negative in western hemisphere)

LON = longitude of site, °E of Greenwich

n = day of the year

N = number of days

q = heat transfer rate, W

$SkyEF$ = sky exposure factor, ratio of exposure to entire sky

T_θ = spectral transmittance of glazing system

N_θ = Inward flowing fraction x spectral absorptance of glazing system

T_b = air temperature at base or ground level, °C

T_e = sol-air temperature, °C

T_o = outdoor air temperature, °C

T_z = air temperature at altitude z, °C

U = U-value, W/m²K

WWR = window wall ratio

X = outdoor air temperature recorded by meteorological station, °C

z = altitude, m

ΔR = difference between long-wave radiation incident on surface from sky and surroundings and radiation emitted by blackbody at outdoor air temperature, W/m²

i   = inside surface

o   = outside surface

t   = hour

d   = day

m   = month

Chapter 1 Introduction

1.1 Research problem

Energy scarcity has been a problem the world has seen for many years. With increasing urbanization, more emphasis should be placed on the search for methods of energy conservation in the building sector. Statistics further affirms this when it was reported that buildings account for 40% of global energy use with resulting carbon emission that are substantially more compared to the transport sector (WBCSD 2009). Increasing urbanization causes the deterioration of the urban environment, as the size of housing plots decreases, thus increasing densities and crowding out greeneries (Santamouris, et al. 2001). As a result, cities tend to record higher temperatures than their non-urbanized surroundings, a phenomenon known as Urban Heat Island (UHI) (Oke 1982; Jusuf, et al. 2007). The distribution of ambient air temperature in an urban canyon greatly affects the energy consumption of buildings. Higher temperatures result in increased heat conducted through a building's envelope, thus increasing cooling energy in a building which forms a significant proportion of the energy used in a building, particularly in places with a tropical climate. In addition, shading effects by surrounding buildings are usually not accounted for when evaluating building performance. Given that 52% of energy consumed in a typical commercial building in Singapore is for air conditioning (Lee, et al. 2004), it is beneficial if the evaluation of an urban environment can be extended to include its impact on buildings. To be useful to most urban planners, the tool must also not require an extensive technical background and should make use of readily available information.

1.2 Scope

The scope of this study is restricted to commercial office buildings in Singapore's Central Business District (CBD), namely along Shenton Way and Tanjong Pagar to keep it manageable. For this study, the heat fluxes into the building being considered are the increase in heat conduction across the opaque wall (δq_{wall}), fenestration (δq_{win}) and the roof (δq_{roof}) brought about due to difference in a building's surrounding (UHI effect). The study also evaluates the amount of solar heat gain through glazing, taking into account shading effects by a building's surrounding. It should be noted that the study does not have a fully diagnostic aim, but instead to provide a methodology that is capable of providing comparative figures/illustration of envelope performance across buildings in the CBD of Singapore.

1.3 Objectives

The objective of this study is to develop a simple method that predicts the envelope performance of commercial office buildings in Singapore, taking into account the local urban microclimate. This includes the development of a method for converting the output from urban microclimate models into a complete year of hourly weather data. The aim is to develop a tool that makes use of readily available data for use by urban planners and policy making, to guide and evaluate an estate's environmental condition while taking into account the building's façade performance and its surrounding urban parameters.

1.4 Organization of study

Chapter 2 reviews the literature

The methodology is given in Chapter 3. Temperature measurements were collected along Shenton Way and Tanjong Pagar in the Central Business District of Singapore. This data was used to develop an empirical model that calculates a 24 hour profile of the urban microclimate temperature using weather data from Singapore's meteorological station as an input.

Building data for 25 commercial office buildings in the central business districted were provided by the Building and Construction Authority of Singapore. This data was used to generalize various building envelope construction in Singapore and used as input to IES-VE® (Integrated Environmental Solutions) virtual environment building performance simulation software. Chapter 3 also describes the models used to calculate the changes in conduction gains through the building envelope and the absolute solar heat gain through glazing.

The model is refined in Chapter 4 using least squares estimation and the data analyzed by making a comparison between the model output with that generated by the simulation software using weather data measured using the weather stations that were deployed along Shenton Way and Tanjong Pagar. Analysis was done to compare results from the simulations and those calculated using the conduction gain models and the solar heat gain model.

Chapter 5 describes the application using 8 buildings located in the Central Business District of Singapore. Detailed materials and construction of the building's facade are used to evaluate their performance. The results are analysed and discussed.

The final chapter concludes the study and provides recommendation.

Chapter 2 Literature review

2.1 Conduction processes

Conduction through a wall or fenestration is time dependent and the process can be represented with a thermal circuit diagram (Figure 2.1). As illustrated in figure 2.1, most heat transfer problems usually involves more than one heat transfer coefficient. Solving for conductive gain using the heat balance method would therefore involve solving the heat flux and temperature of the inside and outside surface simultaneously.
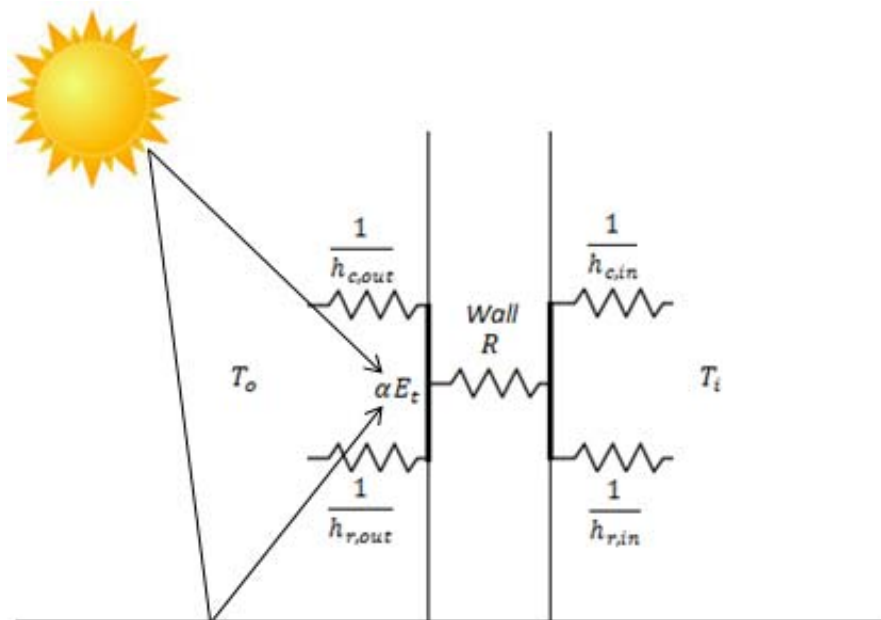
Figure 2.1 Thermal circuit for conduction process through wall

To simplify this process, some models have included the surface heat transfer coefficients as part of the wall element. These various heat transfer coefficient are combined into an overall coefficient (U-value) so that the total conductive gain can be quantified based on the temperature gradient of the outdoor and indoor air temperature instead of surface temperatures as shown in equation 2.1 and 2.2 below. This however, may reduce its accuracy since it assumes a constant value for the heat transfer coefficients although they are prone changes as airflow and temperature

changes. This is particularly true for outdoor surface heat transfer coefficients which are exposed to constantly changing weather conditions.

$$q = U \, A \, (T_o - T_i) \cdots (2.1)$$

$$U = \left(\frac{1}{h_{c,o} + h_{r,o}} + \frac{1}{h_{c,o} + h_{r,i}} + \frac{Length}{k} \right)^{-1} \cdots (2.2)$$

2.1.1 Sol-air Temperature

The sol-air temperature was introduced so that equation 2.2 above may better approximate conduction gain. (ASHRAE 2009) defines it as the outdoor air temperature that, in the absence of all radiation changes gives the same rate of heat entry into the surface as would the combination of incident solar ration, radiant energy exchange with the sky and other outdoor surroundings, and convective heat exchange with outdoor air and it is expressed using equation 2.3 below.

$$T_e = T_o + \frac{\alpha E_t}{h_o} - \frac{\varepsilon \Delta R}{h_o} \cdots (2.3)$$

For horizontal roofs that receive long-wave radiation from the sky only, ΔR can be approximated with a value of $63W/m^2$ (ASHRAE 2009). For walls and fenestration, ΔR is usually assumed to take the value of zero. This is because vertical surfaces receive long-wave radiation from the ground, its surrounding and the sky. When solar radiation intensity is high, which is usually the case in Singapore; surfaces in urban areas usually record a higher temperature then the outdoor air. As a result, their long wave component compensates to a certain extent for the sky's low emittance. The other variables in equation 2.3 can either be obtained from the weather station or calculated based on weather data, making it easy to make an analysis.

2.1.2 Solar radiation through windows

Singapore's hot and humid climate is characterised by small seasonal variations in temperature and relative humidity. This is due to its low latitude of 1.37°. Furthermore, as Singapore is located close to the equator, overheating due to solar radiation occurs all year round, making them undesirable. Studies have also shown solar radiation gains through windows to be a significant contributor to the cooling load of commercial offices in Singapore (Chou and Lee 1988; Chua and Chou 2010). Hence it is important that solar radiation calculations be included when evaluating the performance of building enclosures.

Total solar heat gain through a window has two components, the directly transmitted solar radiation and the inward flowing portion of the absorbed solar radiation. These components depend on the overall transmittance and the absorptance of the window which changes as a function of the angle of incidence. The directly transmitted portion is calculated by multiplying the incident radiation by the glazing area and its solar transmittance. A hemispherical average transmittance value also referred to as the solar heat gain coefficient (SHGC) or g-value is usually used to account for the diffuse sky radiation and radiation reflected from the ground. Generally, as the angle of incidence increases from zero to ninety degrees, transmittance decreases, reflectance increases, and absorptance first increases due to the lengthened optical path and subsequently decreases as more incident radiation gets reflected (ASHRAE 2009). Although these properties are required for all angle of incidence, they are usually only supplied at the normal angle of incidence or zero degrees. Although the principles for calculating solar heat gain through fenestration is well established, it is very time consuming to repeat 'exact' Fresnel calculations (Born and Wolf 1999). Therefore, in practice, the rating of glazing is usually greatly simplified.

The use of normal incidence SHGC, g-value or SC to rate and characterize windows however is not sufficient for determining solar heat gains, since spectral properties of glazing elements varies with angle of incidence. This is especially so with certain types of glazing such as heat absorbing and double glazing, where the use of a constant SC or SHGC value can lead to intolerable errors when estimating the amount of solar heat gain through windows (El-Asfouri, et al. 1988). Hence, to be representative, solar heat gain needs to be calculated as a function of the incident solar angle which changes with time and location. This angular dependence can be easily accounted for in direct or beam solar radiation, because beam radiation is incident from a single easily determined direction. Diffuse and ground reflected radiation however is more complicated since each individual energy flows caused by these components come from multiple directions. Although they can be calculated for a particular sky condition using detailed sky models, the labour involved makes such calculation impractical for building load estimation. As a result, diffuse radiation from the sky and ground are usually assumed to be ideally diffuse by integrating over all directions.

2.1.3 Interrelation between diffuse and global radiation

It is important to note that to quantify the total incident solar radiation requires the direct and diffuse components to be distinguished. Most meteorological stations however only records global solar radiation. In order to determine the magnitude of direct and diffuse solar radiation, empirical correlations can be employed. Using measured data from Blue Hill, Massachusetts in the United States, (Liu and Jordan 1960) were the first to present significant relationship between gobal solar radiation and its diffuse components. Based on data from four weather stations in Canada, (Ruth and Chant 1976) extended the conclusion and showed that although the

correlations provided an excellent method for estimating the diffuse components, they were latitude dependant and not generally applicable. Therefore to be applicable for use in Singapore, (Hawlader 1984) using previously measured weather data in comparison with hourly global radiation recorded by the Meteorological Stations in Singapore, developed correlations for separating the diffuse component from measured values of global radiation. These correlations are shown in equations 2.4 to 2.6 below.

$$(K_d)_t = 1.1389 - 0.9422(K_T)_t - 0.3878(K_T)_t^2$$

$$for\ 0.225 \leq (K_T)_t \leq 0.775 \cdots (2.4)$$

$$(K_d)_t = 0.915\ for\ 0 \leq (K_T)_t < 0.225 \cdots (2.5)$$

$$(K_d)_t = 0.215\ for\ (K_T)_t > 0.775 \cdots (2.6)$$

2.1.6 Code for envelope performance in Singapore

Adopted by Singapore Building and Construction Authority (BCA), the ETTV and RTTV is now widely used in Singapore as an indicator of building performance and air-conditioned commercial buildings are mandated not to exceed a value of 50W/m². Developed in the 1980s by(Chou and Chang 1993), the ETTV/RTTV takes into account the major heat transfers between a building and its surrounding. Its formulation is shown in equations 2.7 and 2.8 below. The heat transfer components accounted for includes conduction through walls, windows and roofs, and radiative heat gain through windows. These were formulated using a generic office building modelled in DOE-2 to calculate a series of weather dependent coefficients (numerical values on RHS of equations 2.7 and 2.8) for each of the above mentioned heat transfer component. The ETTV and RTTV formulation is derived based on equations 2.1 and

2.2 above and assumes an outside and inside surface resistance of 0.044m²k/W and 0.12m²k/W respectively. It has been validated using building energy modelling program DOE-2 developed by the U.S Department of Energy. However, because these weather dependent coefficients were derived based on simulations run using current weather data obtained from meteorological stations, they are likely to vary according to variations in air temperature due to different microclimatic conditions; resulting in overestimation of a building's performance should the effects of urban heat island be considered.

$$ETTV = 12(1 - WWR)U_w + 3.4(WWR)U_f + 211(WWR)(CF)(SC) \cdots (2.7)$$

$$RTTV = 12.5(1 - SKR)U_r + 4.8(SKR)U_s + 485(SKR)(CF)(SC) \cdots (2.8)$$

It should also be noted that most current works aimed at estimating cooling energy consumption or building envelope performance usually assumes that external weather conditions are similar regardless of surface modifications and do not account for the effect urban heat island might have on meteorological conditions and energy use.

2.2 Urban climate analysis and its impacts on envelope performance

2.2.1 Climatic mapping and Geographical Information System (GIS) for urban planning

Over recent years, climatic mapping has been increasingly used for urban planning because of its ability to provide a macro overview which is necessary if the physical development of an urban landscape is to proceed in a sustainable manner. Using GIS, different information could be integrated and laid over one another, providing a clearer picture for analysis and comparison. Using a GIS-based simulation approach, (Chen and Ng 2011) quantified UHI and wind dynamic characteristics of the urban environment from SVF (Sky View Factor) and FAD (Frontal Area Density) simulation respectively. These results are then integrated into a climatic map and used to quantify and address concerns on human thermal comfort in an urban environment.

(Kinya and Koumura 2003) extracted the current greenery distribution in Japan through image processing of ADS40 image data. By overlaying this measured data together with the building shape data in GIS, they were able to determine possible spaces for rooftop greening and set realistic target values for greening. Similarly, by overlaying mobile survey measurements and thermal satellite images with land use maps respectively, (Jusuf, et al. 2007)was able to analyse and compare the temperature profiles for different land use during day and night time.

In another study of a larger scale, (Katzschner and MÜlder 2008) utilized GIS to combine land use data, topographical information and climatic data at a regional level. Through GIS, they were able to generate a climate map which contains information on thermal comfort, microclimatic conditions and ventilation patterns, and provide recommendations to support the development plans of different villages.

Till date however, few have related the impact of microclimatic conditions to building envelope performance. Although (Kikegawa, et al. 2003) and (Salamanca, et al. 2009) have integrated building energy models with urban canopy models, these numerical models may be difficult to use for the non-technical user. Furthermore, they may be time-consuming, particularly when evaluating a significantly large area or when the aim is to provide a macro overview of different possible development plans.

2.2.2 Parameters affecting envelope thermal performance

The amount of heat gained or lost through a building envelope is not only dependent on the immediate properties of the envelope (such as built form, surface to volume ratio, U-value, glazing ratio, material emissivity and reflectance, etc), but also on the ambient conditions surrounding it. These ambient conditions can be categorized into internal and external. Internal conditions are typically determined by the setpoint temperature and various internal gains. External conditions on the other hand are more complicated and may vary depending on the urban morphology surrounding the building. This has been reaffirmed by (Jusuf, et al. 2007) who concluded that temperature patterns in Singapore are closely related to urban land use. Typically, parameters that have been found to have an impact on urban air temperature include the amount of greenery, height of buildings and the width of the urban canopy. It is the interaction between exposed urban surfaces and the ambient conditions that forms the basis of urban climate models that has been used to calculate the microclimate air temperature in an urban estate.

One way to quantify this variation in external ambient air temperature is through the use of Screening Tool for Estate Environment Evaluation (STEVE) tool. STEVE tool is an empirical model that calculates the maximum, minimum and average air

temperature of a point of interest based on a 50m radius in an urban built up area in Singapore. The use of 50m radius was based on a preliminary study by (Jusuf and Wong 2009) which found that a 50m radius amongst a range of 25 to 100m (at 25m intervals), best explains the impact of urban morphology on air temperature in Singapore (Figure 2.3). This result is closely similar to another study by (Kruger and Givoni 2007) which concluded that land features within a 56m had a better correlation with the urban air temperature as compared to 125 and 565m based on data from seven weather stations in Brazil.
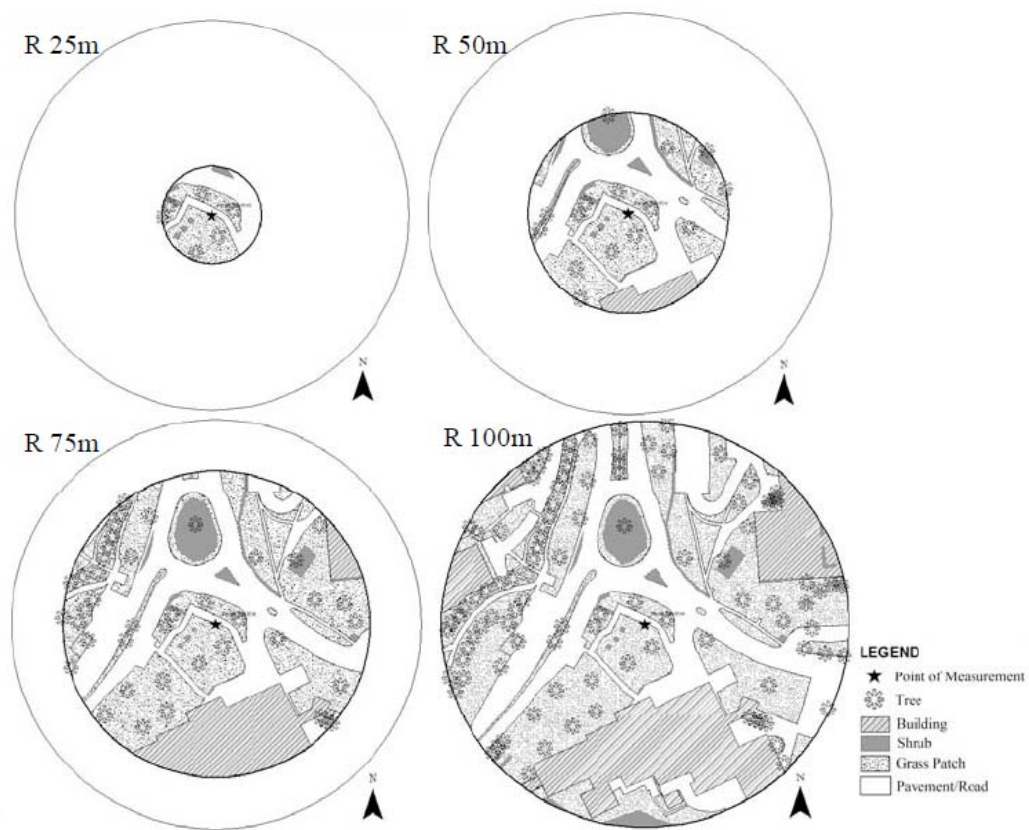

Figure 2.2 Preliminary study to determine radius of influence (Jusuf and Wong 2009)

The output of STEVE tool is based on a regression model that has various urban morphology and climate predictors as independent variables. These prediction models were formulated based on data collected over a period of close to 3 years at various

location within the NUS Kent Ridge Campus and One North (Wong and Jusuf 2008; Wong and Jusuf 2008). The independent variables of this model can be divided into two categories as follow:

1. Climate predictors: daily minimum, maximum and average air temperatures; daily average solar radiation; all these climate predictors are obtained from the meteorological station.

2. Predictors of urban morphology: percentage of pavement over a 50m radius; average height to building area ratio; total wall surface area; green plot ratio; sky view factor; and average surface albedo. The green plot ratio is derived using the leaf area index in proportion to the total lot area. The higher the green plot ratio, the denser the greenery condition in a built environment (Ong 2003).

However, as the tool only predicts the minimum, maximum and average air temperatures due to UHI effect, it is not suitable for use in building energy simulation programmes that require hourly weather data to run. This was also the motivation behind developing an empirical model that is able to calculate a 24 hour profile for a typical day of each of the 12 months in a year based on the minimum, average and maximum temperatures.

Chapter 3 Methodology

Figure 3.1 below illustrates the overview workflow to producing a climatic map which is a representation of the ambient air temperature due to UHI effect while also illustrating its impact on building enclosures.
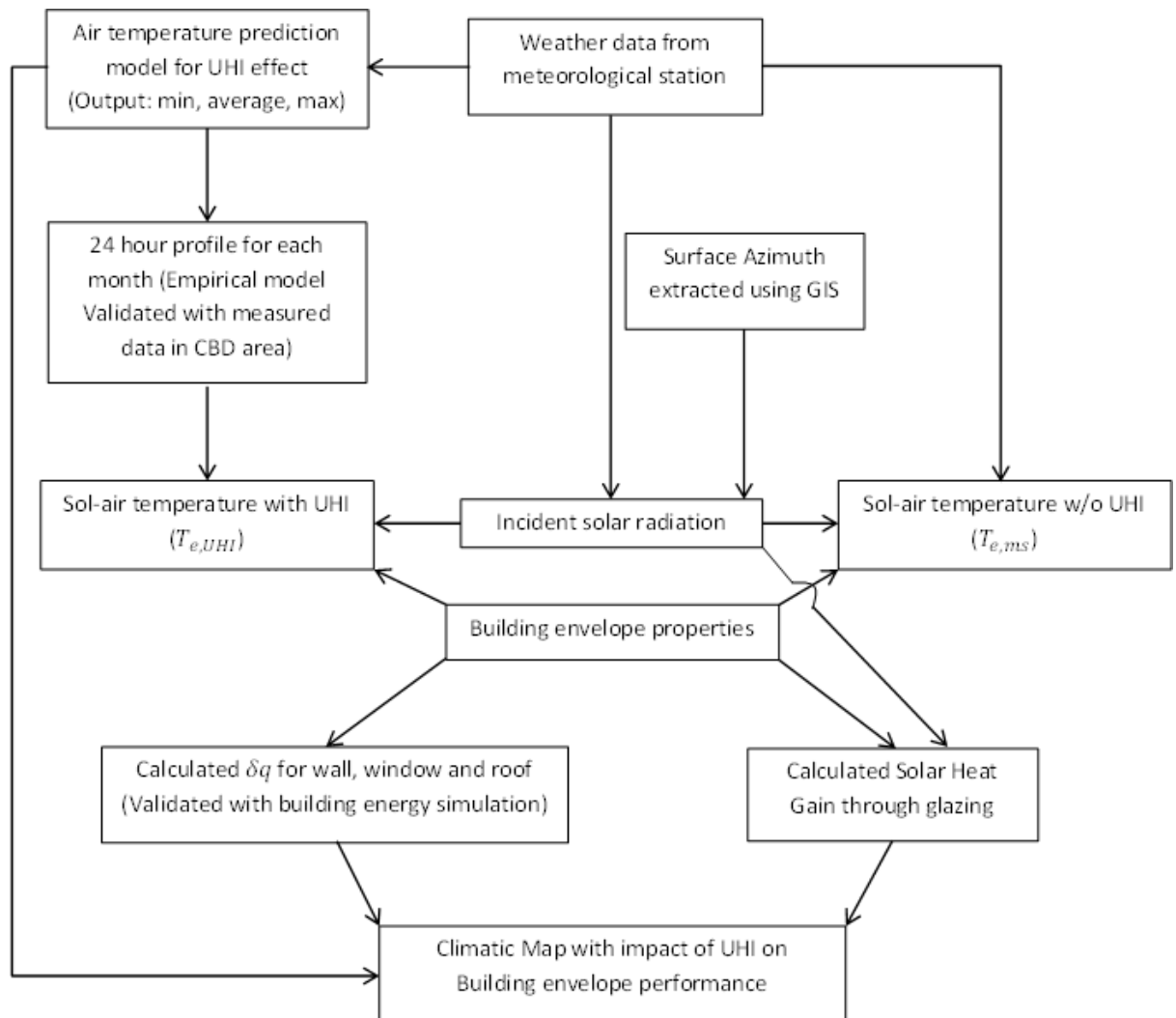

Figure 3.1 Approach to climate impact assessment with impact on building envelope

3.1 Local outdoor air temperature calculation

Hourly weather data are required as input to predict the performance of a building's enclosure. Hence, to account for the impact of UHI effect on envelope performance, a method needs to be developed for using maximum, minimum and average temperature (the output of STEVE tool) to produce a 24 hour profile.

Temperature measurements were conducted along Shenton Way and Tanjong Pagar in the Central Business District of Singapore (Figure 3.2). The equipment used for measurement is the HOBO data logger U12-011 and is housed inside solar cover to protect it from direct solar radiation. The HOBO U12has a measurement range of -20°C to 70°C and has an accuracy of ±0.35°C for temperatures between 0°C to 50°C. Temperatures were recorded at one minute intervals for a period of approximately two months (March and April 2012). Measured data from March 2012 and April 2012 were compared with temperatures recorded at Singapore's meteorological station at Sentosa to develop an empirical model (Equations 3.1 to 3.3) that is capable of generating a 24 hour profile for a typical day of each month in a year. Equations 3.1 to 3.3 are original work. It is important to note that the modified weather data represents typical rather than extreme weather conditions.

If $X_t < X_{avg}$,

$$T_t = T_{min} + (X_t - X_{min}) \frac{(X_{max} - X_{min})}{(X_{avg} - X_{min})^2} \frac{(T_{avg} - T_{min})^2}{(T_{max} - T_{min})} \cdots (3.1)$$

If $X_t > X_{avg}$,

$$T_t = T_{max} - (X_{max} - X_t) \frac{(X_{max} - X_{min})}{(X_{max} - X_{avg})^2} \frac{(T_{max} - T_{avg})^2}{(T_{max} - T_{min})} \cdots (3.2)$$

$$X_t = \langle X_t \rangle_m = \frac{1}{N} \sum_{Day\ d=1,}^{N=number\ of\ days\ in\ month\ m} X_t \cdots (3.3)$$

N is the number of days in $month\ m$ and $X_{d,t}$ is air temperature recorded by the meteorological station on $day\ d$ at $hour\ t$. X_t also denoted by $\langle X_t \rangle_m$ is defined to be the variable X_t averaged over the number of days N for each $hour\ t$ in $month\ m$, generating a 24 hour profile of averages. For instance, $\langle X_1 \rangle_2$ represents the average of all air temperatures recorded at Singapore's meteorological station at 1 in the morning in the month of February. X_{min}, X_{avg} and X_{max} represent the average (minimum, average and maximum) temperatures recorded at the meteorological station respectively during $month\ m$. X_{min}, X_{avg} and X_{max} were then used as input into STEVE to calculate T_{min}, T_{avg} and T_{max} respectively. These are the average (minimum, average and maximum) temperatures predicted for various points in an urban estate, after considering the surrounding morphology of a building.

Variation in outdoor air temperature with altitude is accounted for and calculated using the (ICAO Standard Atmosphere 1964) and is similar to the molecular-scale temperature model used in building energy simulation program EnergyPlus (UIUC and LBNL 2011). According to this model, the variations in air temperature can be defined by a series of connected segments that are linear in geopotential altitude up to 32km. For the purpose of modelling buildings, we need only be concerned with variations in the troposphere which can be defined by equation 3.4 below.

$$T_z = T_b + L(H_z - H_b) \cdots (3.4)$$

The gradient of air temperature L is equal to a rate of -6.5 K/km up to a geopotential altitude of 11km (U.S. Standard Atmosphere 1976). The geopotential altitude H_z and

geometric altitude z are almost the same in the lower atmosphere and can be calculated by equation 3.5(UIUC and LBNL 2011). Geometric altitude is defined as the height above ground level and the geopotential altitude at ground level H_b is equal to zero.

$$H_z = \frac{E \times z}{(E + z)} \cdots (3.5)$$

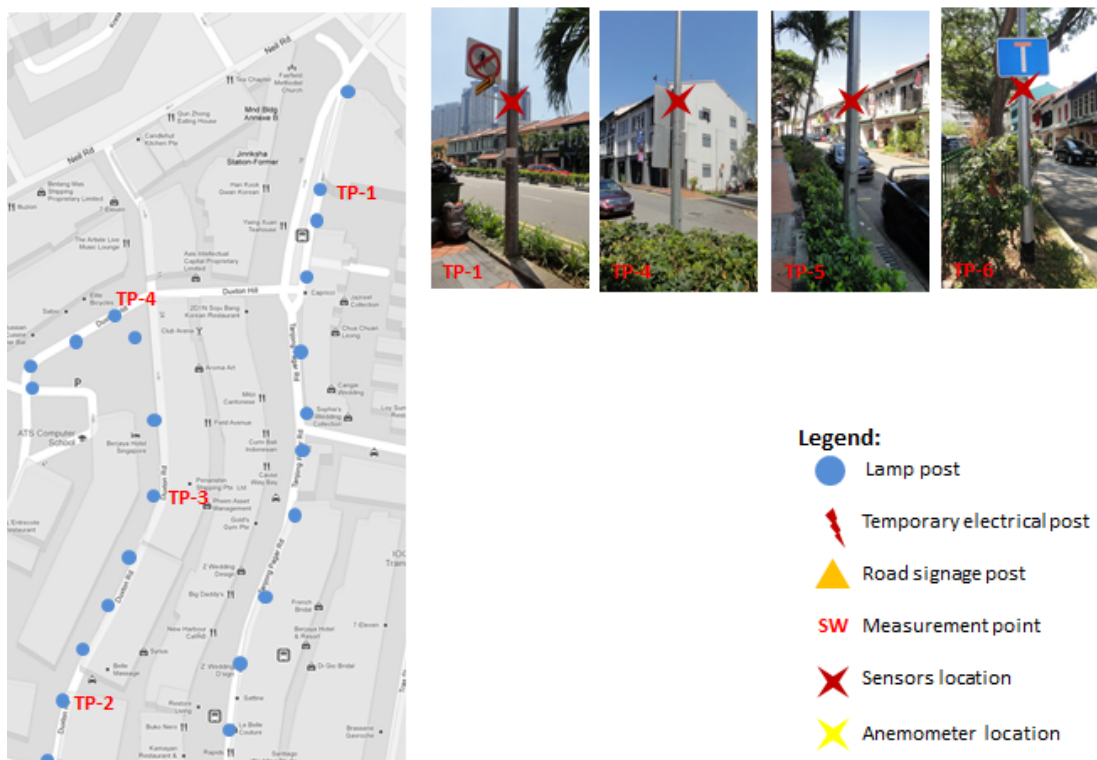Since air temperatures are usually measured about 1.5 meters above ground level, air temperature at ground level, T_b can be derived by inverting equation 3.4 to give equation 3.6. At 1.5 meters above ground level, $T_b = T_{z,1.5} + 6.5(0.0015)$.

$$T_b = T_{z,met} + 6.5(\frac{E \times z_{met}}{E + z_{met}} - H_b) \cdots (3.6)$$
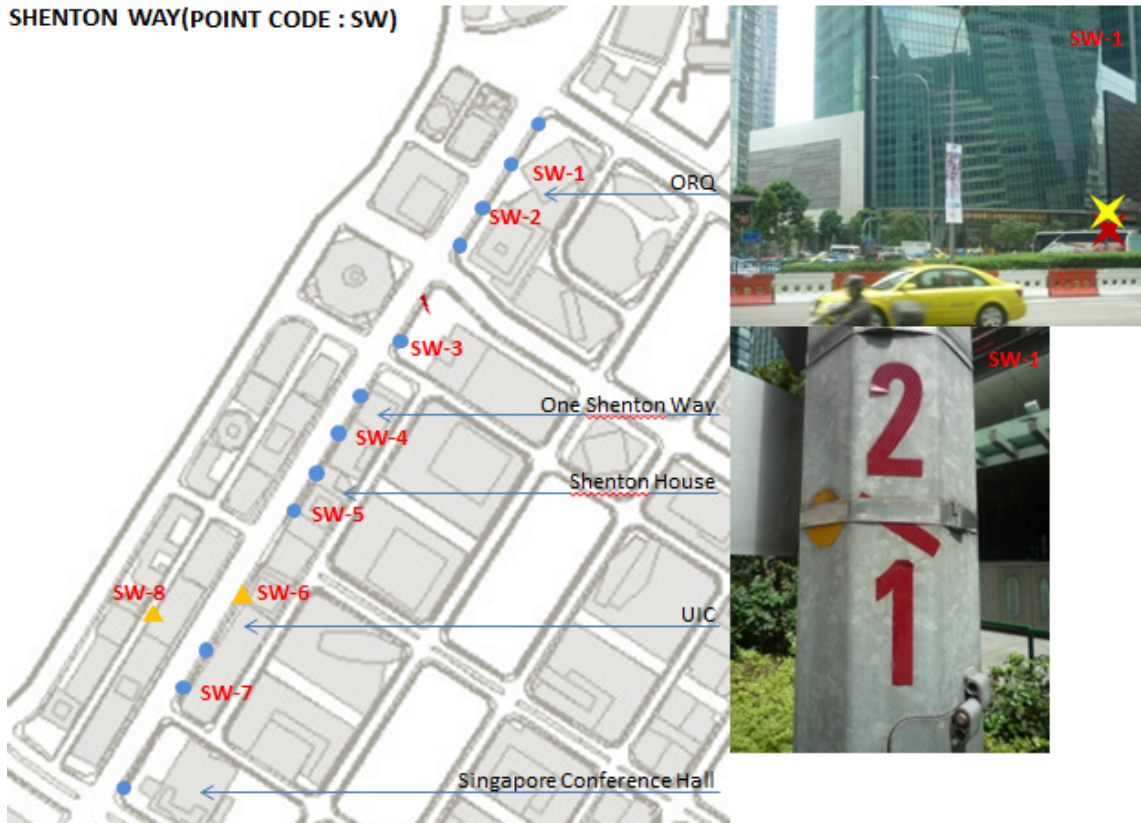
Figure 3.2 Measurement points in Central Business District, Singapore

3.2 Conduction gain through exterior surfaces

Conduction through exterior walls, windows and roofs is calculated using the sol-air temperature defined by equation 2.3 in Chapter 2 in conjunction with the familiar conduction equation (Equation 3.7). This is calculated for each hour, t over the 24 hour profile calculated for each month using equations 3.1 to 3.3 above. To better account for changes in outside surface heat transfer coefficients, equation 3.8 is used to calculate the sol-air temperature instead. Both $T_{o,t}$ and $E_{T,t}$ represent the outdoor temperature and total incident solar radiation averaged over the month for hour t respectively.

$$q_{cond,t} = UA(T_{e,t} - T_{i,t}) \cdots (3.7)$$

$$T_{e,t} = T_{o,t} + \frac{\alpha E_{T,t}}{h_{r,t} + h_c} - \frac{\varepsilon \Delta R}{h_{r,t} + h_c} \cdots (3.8)$$

$$h_{r,t} = 4\varepsilon\sigma(\frac{T_{e,t} + T_{o,t}}{2})^3 \cdots (3.9)$$

A linearized model for calculating the radiation heat transfer coefficient h_r is used (equation 3.9). Equations 3.8 and 3.9 are then solved iteratively to determine the sol-air temperature. Values for h_r are calculated hourly to reflect variations with changing outdoor temperatures. External convective coefficient h_c is assumed to be 14W/m^{2}k, which is a reasonable approximation given Singapore's low wind speed which usually averages below 2m/s.

To simplify the process of evaluating envelope performance, a comparative approach where the change in conduction gain was used to evaluate performance instead of conduction gain itself. Equation 3.7 can therefore be simplified into equation 3.10, where $T_{e,t(UHI)}$ is the sol-air temperature at each hour when UHI effect is considered and $T_{e,t(ms)}$ is the sol-air temperature calculated based on hourly air temperature data

from meteorological services. This simplification also removes dependence on internal setpoint temperature which can have significant impact on conduction gain and may vary from as low as 21°C to as high as 25°C. The difference in gains brought about by UHI is then calculated for each external surface of the building using surface azimuth extracted using GIS and will be explained in greater detail in the next section. In order to provide a more realistic estimation, results from building energy simulation software IES-VE© would be regressed with $UA(T_{e,UHI} - T_{e,ms})$ and least squared estimation used to determine the values of coefficient a and intercept c. This would therefore take into account the effect of other factors that may have an effect on conduction gain based on a typical building in Singapore. This simplification is necessary so that different options or development plans can be considered at a macro scale within reasonable time, while still being sufficiently accurate for an urban planner to make correct choices.

$$\delta q_{cond} = a \sum_{month\ m=1}^{12} \sum_{hour\ t=1}^{24} nUA(T_{e,t(UHI)} - T_{e,t(ms)})_m + c \cdots (3.10)$$

3.3 Incident solar radiation

Incident solar radiation is a required input when calculating the sol-air temperature. The total incident solar radiation is the sum of three components at their respective hour t (Equation 3.11): the beam or direct component from the sun $(E_{b,t})$, the diffuse component from the sky dome $(E_{d,t})$, and the ground-reflected component from solar radiation reflected off the ground onto the receiving surface $(E_{r,t})$. To calculate these parameters, global solar radiation data which is readily available from the meteorological station is first separated into its direct and diffuse components using equations 2.4 to 2.6 (Chapter 2). Each of the components are then calculated using equations 3.12 to 3.14 (ASHRAE 2009; Duffie and Beckman 2006; IES).

$$E_T = E_{b,t} + E_{d,t} + E_{r,t} \cdots (3.11)$$

$$E_{b,t} = E_b \cos\theta \cdots (3.12)$$

$$E_{d,t} = E_d cos^2(\Sigma/2) \cdots (3.13)$$

$$E_{r,t} = \rho(E_b sin\beta + E_d)sin^2(\Sigma/2) \cdots (3.14)$$

The tilt angle Σ, is the inclination of the surface. For the purpose of this study, walls and roofs are assumed to have an angle of 90 and 0 degrees respectively. ρ is the ground reflectance and can be taken to be 0.2 which is typical of surfaces in a city centre (ASHRAE 2009). The value of the incident angle θ depends on geographic latitude, surface azimuth, as well as the time of day and year (Equation 3.15). Equations 3.16 and 3.17 are used to determine the solar altitude β and solar azimuth ɸ respectively (Duffie and Beckman 2006; ASHRAE 2009).

The surface azimuth Ψ can be defined as the orientation of the building where surfaces facing south is taken as 0°. Surfaces to the west have positive values while those to the east are negative. Table 3.1 below shows the surface azimuths for

common orientations of buildings. Using GIS, surface azimuths of different buildings

walls in the CBD area was extracted and used to calculate the incident radiation.

$$\cos\theta = \cos\beta \cos(\varphi - \Psi)\sin\Sigma + \sin\beta \cos\Sigma \cdots (3.15)$$

$$\sin\beta = \cos L \cos\delta \cos\omega + \sin L \sin\delta \cdots (3.16)$$

$$\cos A = sign(\omega)\frac{\cos\omega \cos\delta \sin L - \sin\delta \cos L}{\cos\beta} \cdots (3.17)$$

Where $sign(\omega)$ is +1 when the hour angle is positive and -1 when the hour angle is

negative.

Table 3.1 Common orientations and their azimuths

Orientation	N	NE	E	SE	S	SW	W	NW
surface azimuth Ψ	180°	-135°	-90°	-45°	0°	45°	90°	135°

In order to evaluate the solar altitude and solar azimuth above, the solar declination δ

and hour angle ω was first obtained using equations 3.18 to 3.22 (Duffie and

Beckman 2006; ASHRAE 2009). The local standard time LST in Singapore was

converted to solar time AST using two corrections (Equation 3.20). The first

correction takes into the account the location of the meteorological station and the

meridian on which the local standard time is based. The second correction takes into

account the perturbations in the earth's rate of rotation and is accounted for by the

equation of time (Equation 3.21). The latitude Ψ and longitude LON of Singapore is

1.37 and 103.98 respectively.

$$\delta = 23.45 \sin(360°\frac{284 + n}{365}) \cdots (3.18)$$

$$\omega = 15(AST - 12) \cdots (3.19)$$

$$AST = LST + \frac{ET}{60} + \frac{(LON - LSTM)}{15} \cdots (3.20)$$

$$ET = 2.2918(0.0075 + 0.1868\cos B - 3.2077\sin B - 1.4615\cos 2B$$

$$- 4.089\sin 2B)\cdots(3.21)$$

$$B = 360°\frac{n-1}{365}\cdots(3.22)$$

3.4 Solar heat gain calculation

Transmitted solar radiation is computed at hourly time steps for the entire year and depends on the amount of incident solar radiation. Solar radiation incident on building surfaces can be further broken down into three components; the beam or direct radiation, the diffuse sky radiation, and the ground reflected radiation. As described in the preceding section, the weather file provides global radiation data which are then separated into its direct and diffuse components. These direct and diffuse horizontal radiation fluxes are then used to calculate each of the three components that are incident on every external building surface (equations 3.12 to 3.14).

Instead of using normal incidence solar heat gain coefficient or g-value to calculate total solar heat gains, transmittance and the inward-flowing fractions are computed at ten degree intervals. This is because spectral properties of glazing vary with the angle of incidence. Angular variations in glazing properties are determined using the Fresnel equations (IES). Multiple reflections were considered to determine the portions of incident radiation that are transmitted, absorbed and re-transmitted. These angular and diffuse transmittance values can be easily calculated from computer programs such as WINDOW 5.2 (LBL 2003), or within building energy simulation software IES-VE© using specifications (transmittance and reflectance at normal incidence) that are usually available from glazing catalogues or ASHRAE handbook, fundamentals (ASHRAE 2009). Using IES-VE©, the result is a set of solar

transmission, absorptance and inward-flowing fraction at ten degree intervals. These results were inferred and calculated from normal incidence solar transmission and reflectance of each glazing layer and the resistance provided by any air gaps. Inside and outside convective coefficients were assumed to be constant at 0.05m²K/W and 0.12m²K/W respectively. For simplicity, g-value (BFRC) was used to determine the amount of diffuse sky radiation and ground reflected radiation that enters through the glazing. Since most g-value or SHGC values provided by manufacturers are normal incidence values, the g-values are converted to time-averaged values according to the simplified method used to define g-value (BFRC) (IES; BFRC 2007). Equations 3.24 and 3.25 shows how the diffuse and direct/beam solar heat gain is to be calculated respectively. To account for the shading effect by surrounding buildings in densely built urban centres, the beam or direct component is multiplied by the average Sky Exposure Factor (SkyEF) of the building external surface. SkyEF can be defined as the ratio of the solid angle of the sky patch visible from a certain point on a building's facade to the solid angle of the hemisphere centred at the same point, and represents the "geometric definition" of Sky View Factor (Zhang, et al. 2012). These ratios are then averaged across the building's external surface and applied to equation 3.25. It is multiplied by a factor of 2 because the calculation of SkyEF is based on the ratio of exposure to the entire sky while the ratio of incident direct solar radiation that is not shaded should be based on the ratio from the horizon to the zenith. This is because the amount of direct solar radiation incident on a building surface depends on solar intensity from the horizon to the zenith and does not consider that which is behind the surface.

$$q_{solar,t} = q_{b,t} + q_{d,t} \cdots (3.23)$$

$$q_{d,t} = \left(E_{d,t} + E_{r,t}\right)A(WWR)(g - value) \cdots (3.24)$$

$$q_{b,t} = (2 \times SkyEF)E_{b,t}A(WWR)\left(T_{\theta,t} + N_{\theta,t}\right) \cdots (3.25)$$

Since transmittance and the inward-flowing fractions are determined at ten degree intervals, $T_{\theta,t}$ and $N_{\theta,t}$ were taken as the average of the two spectral values for which the incident angle falls between. For instance, if the angle of incidence fall between 10 and 20 degrees at hour t, $T_{\theta,t}$ would equal the average spectral transmittance values at 10 and 20 degrees.

3.5 Building energy simulation

Since buildings are composed of interdependent subsystems, it is desirable to know the impact on total cooling load in changing several parameters simultaneously. According to (Turiel, et al. 1984), since building energy performance is dependent on many factors, increasing the number of parameters in the analysis greatly improves estimation accuracy. Therefore, for this study, several parameters are varied simultaneously so that the interdependencies between the different parameters are accounted for. A total of 25 commercial office buildings around the central business district in Singapore were surveyed to provide realistic envelope construction and combinations of envelope components. A detailed investigation into their envelope construction produced 27 different generic envelope combinations (Table A.1, Appendix I). Where the detailed roof construction was not available, a typical roof construction for office buildings was applied.

To determine the coefficients of the simple regression model and to determine if solar heat gain calculations were sufficiently accurate, these multiple-parameter variations were carried out using IES-VE© (Integrated Environmental Solutions) virtual environment building performance simulation software which uses the heat balance method described by (ASHRAE 2009) to perform hourly computations of cooling loads components. The building is modelled based on a typical office building design in Singapore. They were assumed to operate on a 55 hour work week which was found to be typical of offices in Singapore (Lee, et al. 2004). The infiltration schedule is the inverse of the cooling schedule because it is assumed that during operation, the building is pressurized and hence no infiltration occurs. Lighting power density and ventilation rates were kept constant at $15w/m^2$ and 0.6 l/s.m² in accordance to codes of practise in Singapore (SS 531 2006; SS 553 2009). Two built forms were considered and they are the pavilion and slab (Figure 3.3). The dimensions were determined by keeping a fixed surface area to volume ratio of 0.15 while keeping the height of the building at 10 storeys with a typical storey height of 3.6m. Ratio of 0.15 was used based on analysis using GIS to extract the volume and corresponding surface area in the CBD area. It was found that 0.15 was the ratio that was the most common.
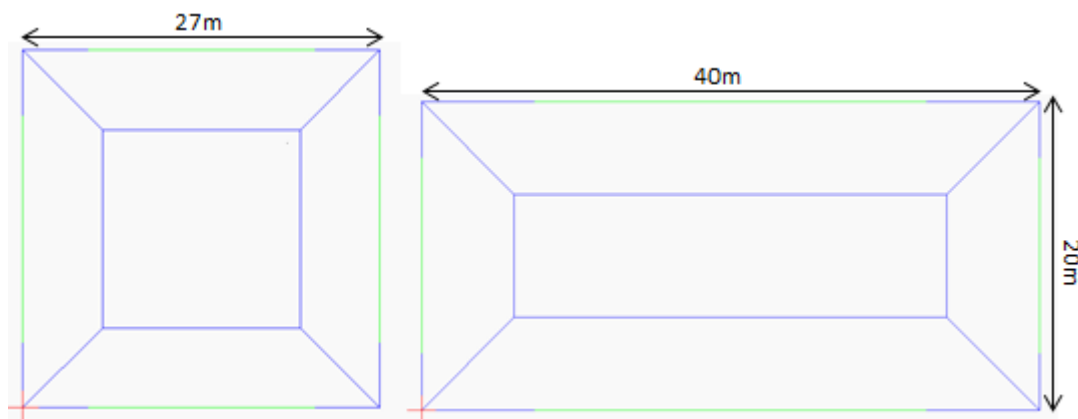

Figure 3.3 Plan view of pavilion and slab built form

To determine the possible change in conduction gains brought about by UHI effect, each built form was assumed to be located along the measurement points illustrated in Figure 3.1 (SW1 to 7 and TP 1 to 4). The modelled buildings were also orientated so that they are aligned with the roads. Each model was run twice, once using weather data from meteorological station and once using temperature measurements conducted along Shenton Way and Tanjong Pagar. The difference was then calculated by subtracting one from the other. The simulations were run from March to April. Using least squared estimation, this difference was correlated with the independent variables in equation 3.10 above to determine the values of coefficient a and intercept c. This was done for conduction gains through walls, windows and roofs respectively. Equation 3.10 was then used to generate a climatic map which includes the impact of UHI on conduction gains through building enclosures using GIS.

The same built forms (Figure 3.2) were used for assessing the solar heat gain calculations. For determining if the solar gain calculations were sufficiently accurate, they were compared to the results provided by the building energy simulation program. The built forms were rotated so that each of the eight surface azimuths (Table 3.1) which represents the general orientations of buildings was accounted for. Each of these cases was then simulated for each of the 26 different generic envelope combinations (Table A.1, Appendix I) and the results compared to the solar heat gain calculated using equations 3.23 to 3.25 described in the preceding section.

Chapter 4 Analysis and validation
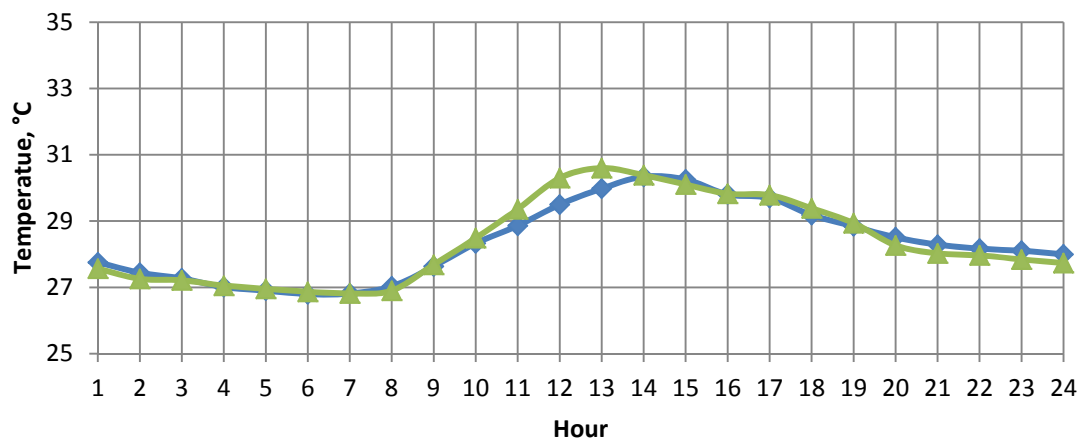
4.1 Calculating 24 hour temperature profile

Figures 4.1 and 4.2 shows the 24 hour temperature profile measured along Shenton Way and Tanjong Pagar (Figure 3.1) against the model output described in Chapter 3.1 taking into consideration the urban morphology surrounding each measurement point. They show the typical 24 profile averaged over the month of March and April respectively. Based on observation of the 24 hour profiles at each measurement point, it can be seen that there is good agreement between modelled and measured data for both March and May. It is important to note that the discrepancies between the maximum and minimum temperatures are most probably brought about due to errors of STEVE tool prediction. This is because according to equation 3.1 and 3.2, where x_t is at minimum or maximum, the predicted temperature T_t equals T_{min} and T_{max} respectively. However, we will show later in this chapter that despite these errors, the model is still able to evaluate the impact of UHI on building envelopes sufficiently accurate for an urban planner to make informed decisions. Another point to note is that temperatures measured in Tanjong Pagar (TP) is slightly higher than points located in Shenton Way (SW). This is due to the fact that building density is higher in Shenton Way, thus provide more shading from direct solar radiation, which explains the lower temperatures in Shenton Way during the afternoon (Jusuf, et al. 2007).
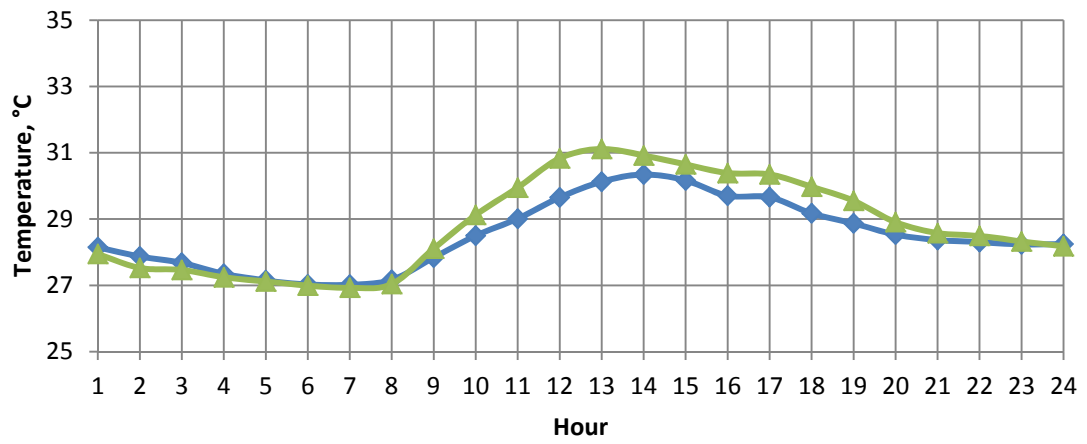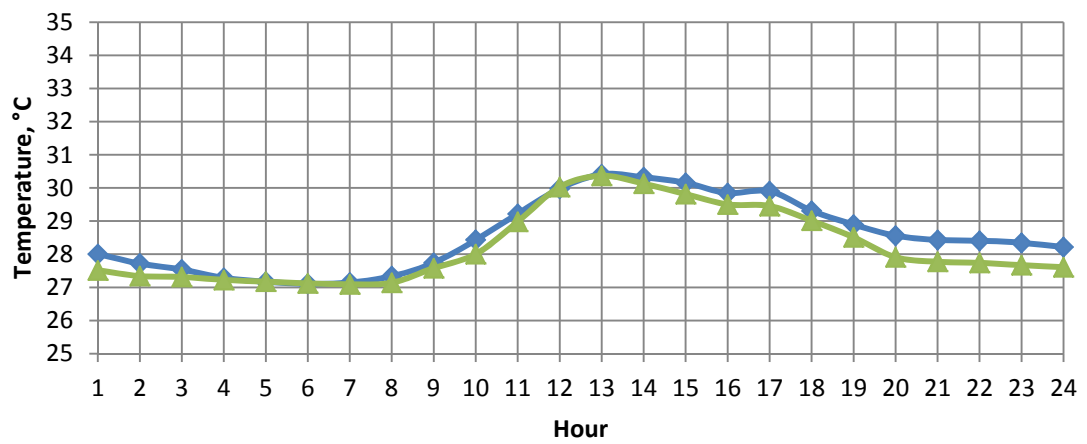
a) SW1

b) SW2

c) SW3

d) SW4

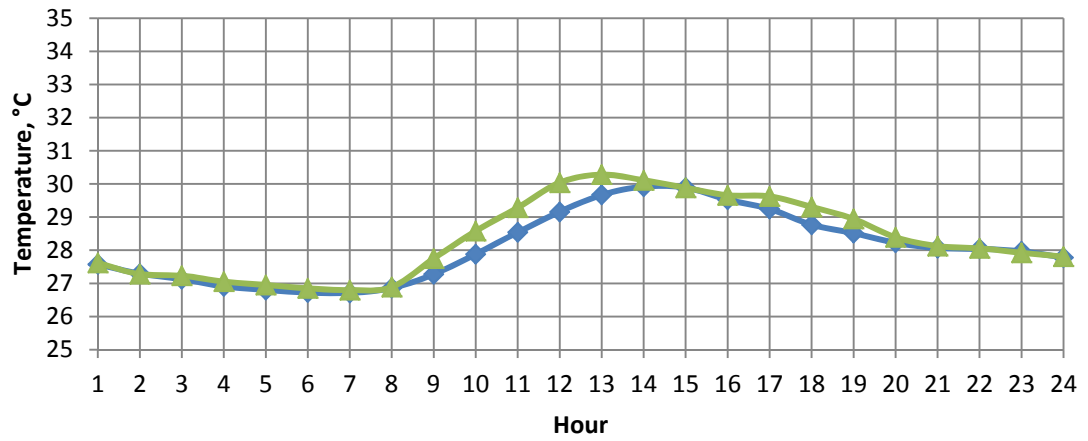**e) SW5**

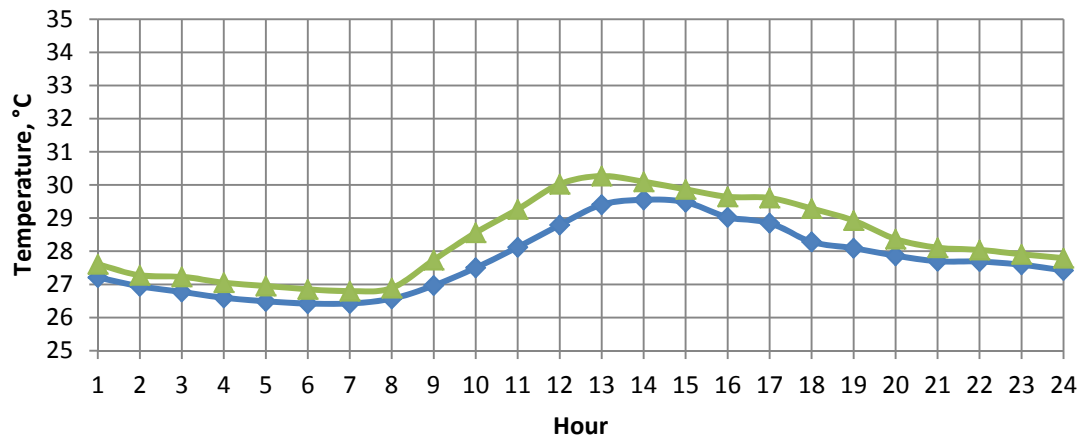**f) SW6**

g) SW7

h) TP1

i) TP2

31

j) TP3

k) TP4
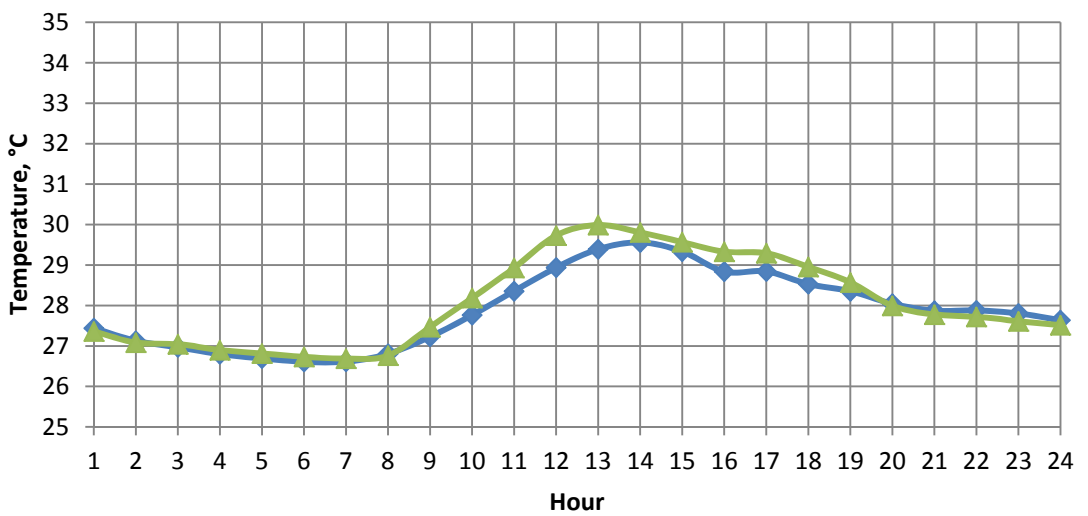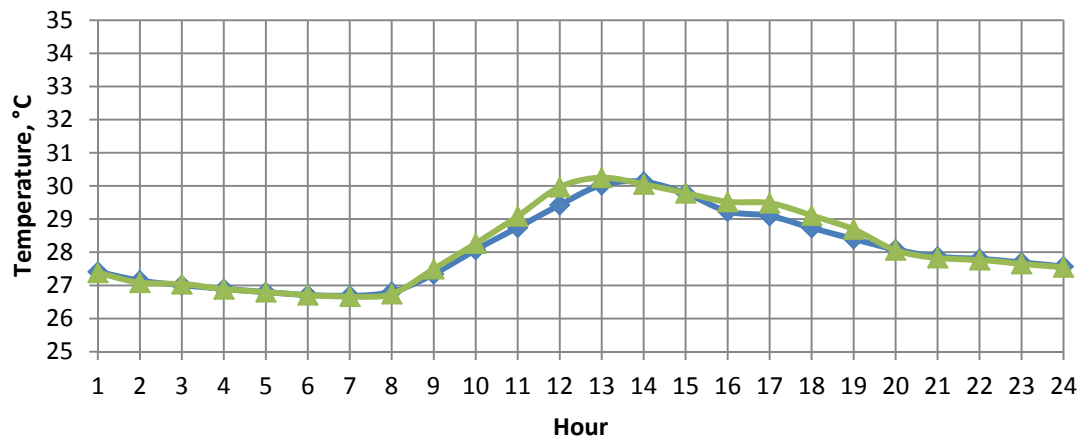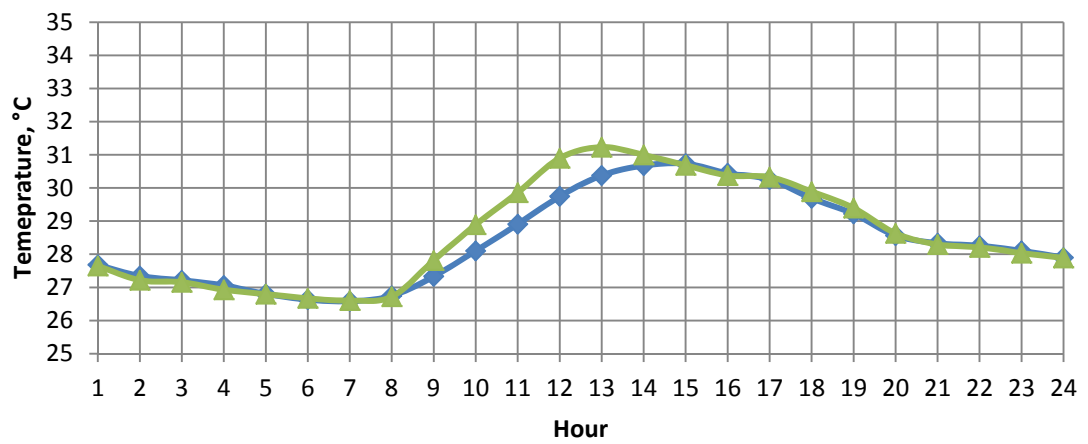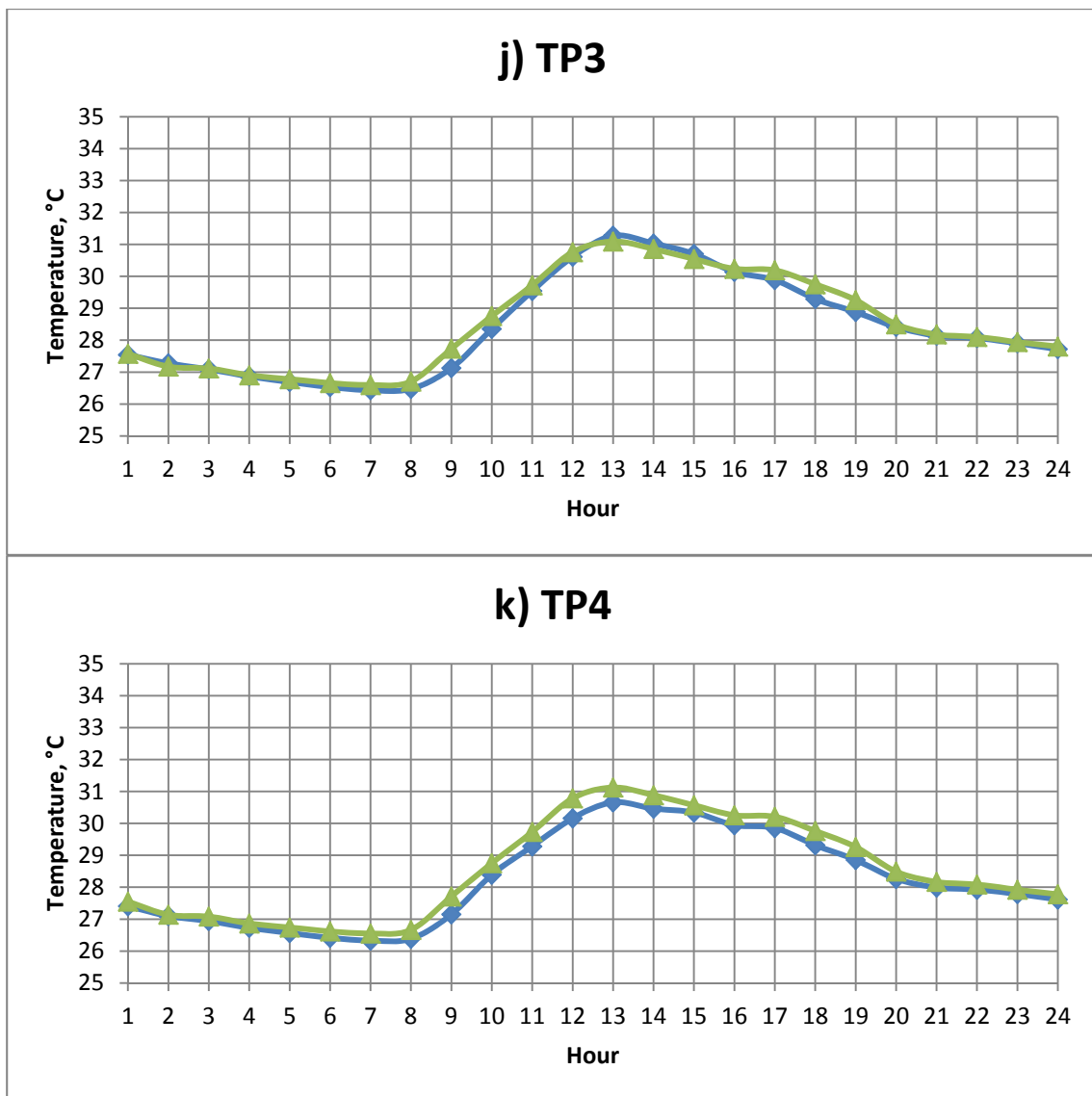
Figure 4.1a-k Modelled versus measured 24 hour temperature profile averaged for March
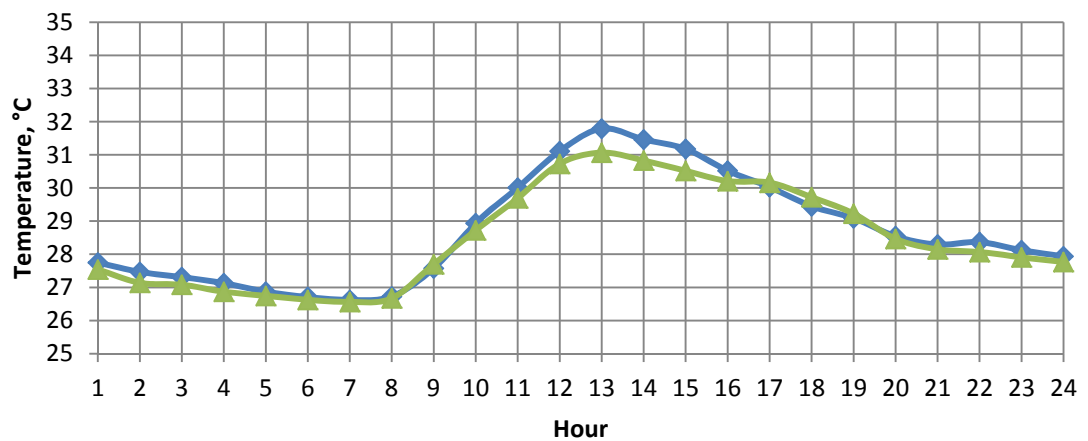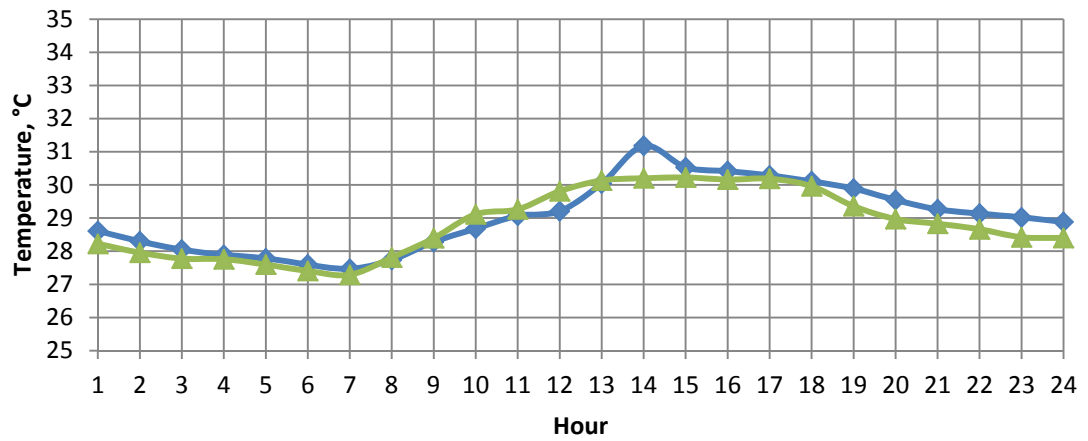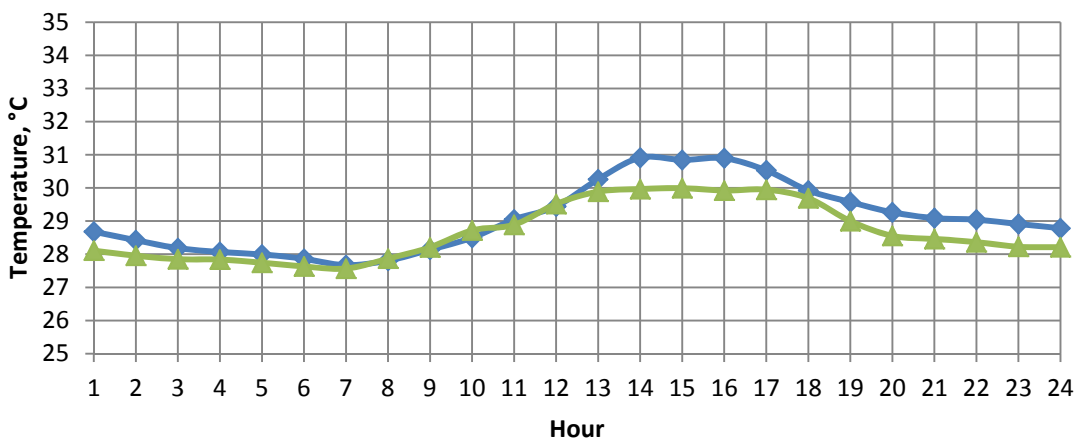
d) SW4
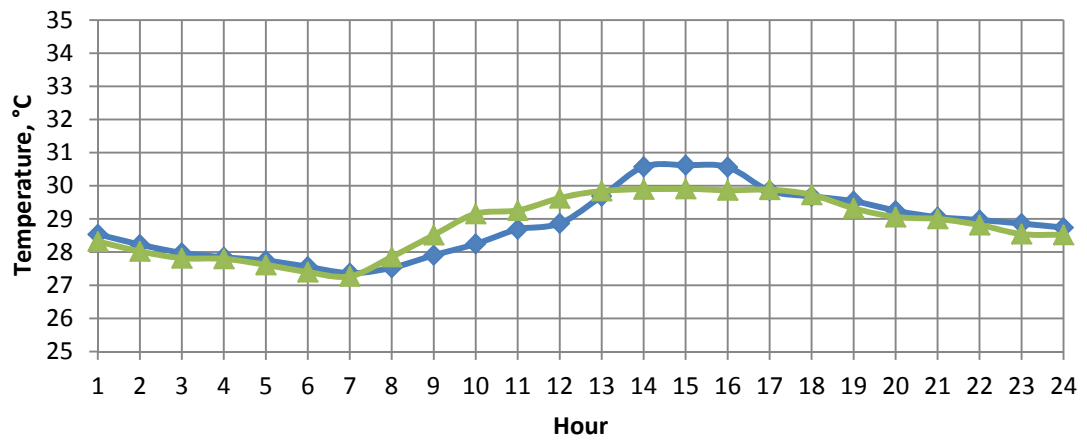
e) SW5
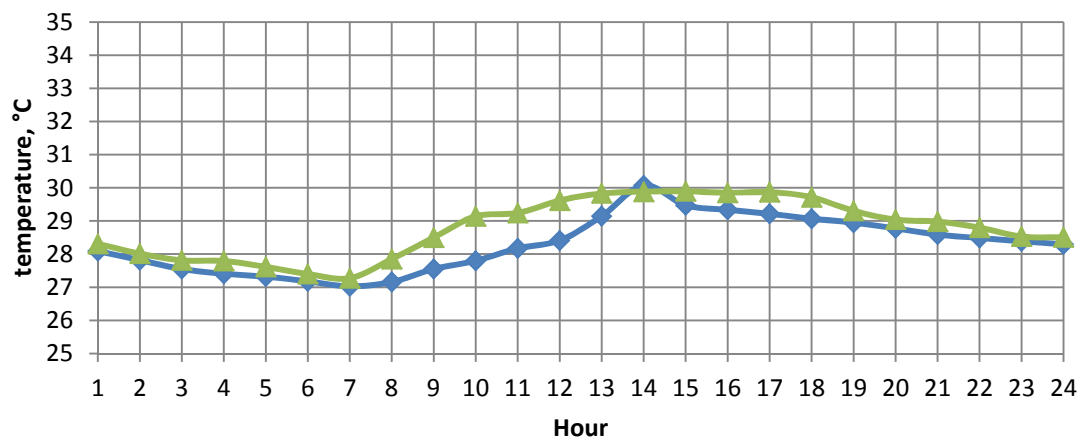
f) SW6
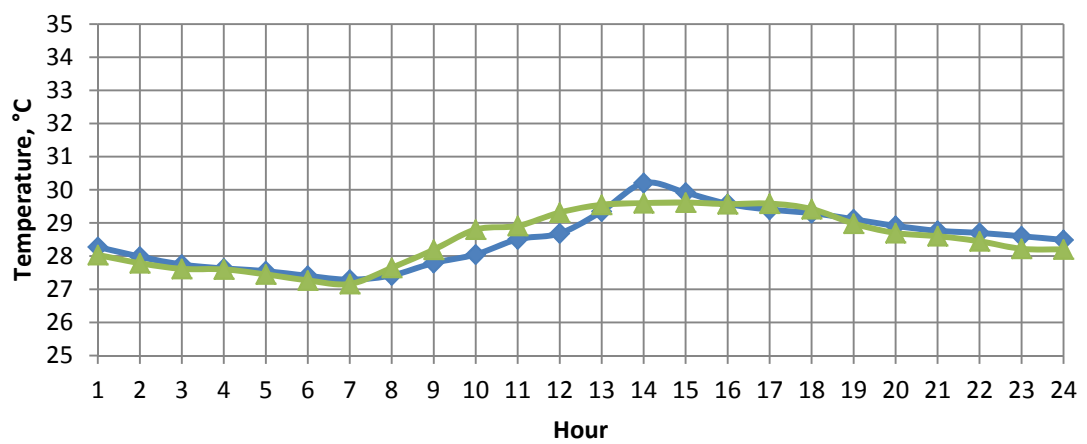
g) SW7
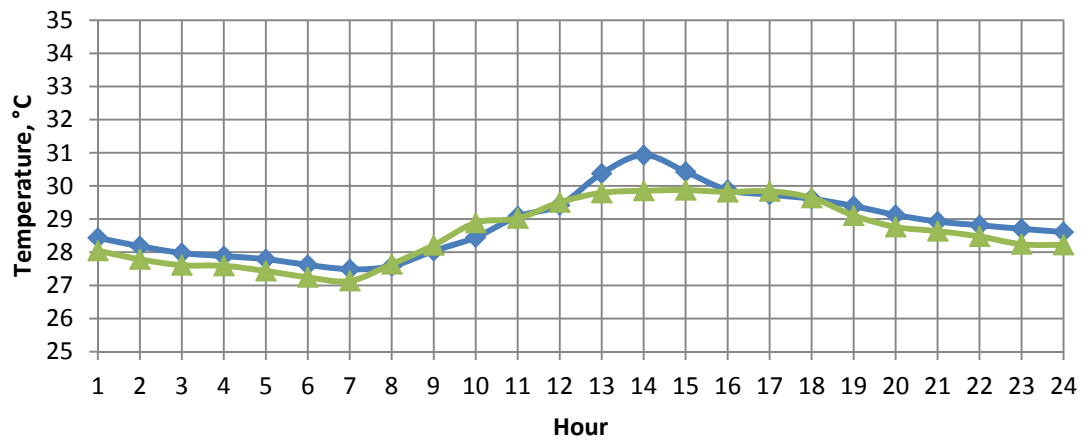
h) TP1
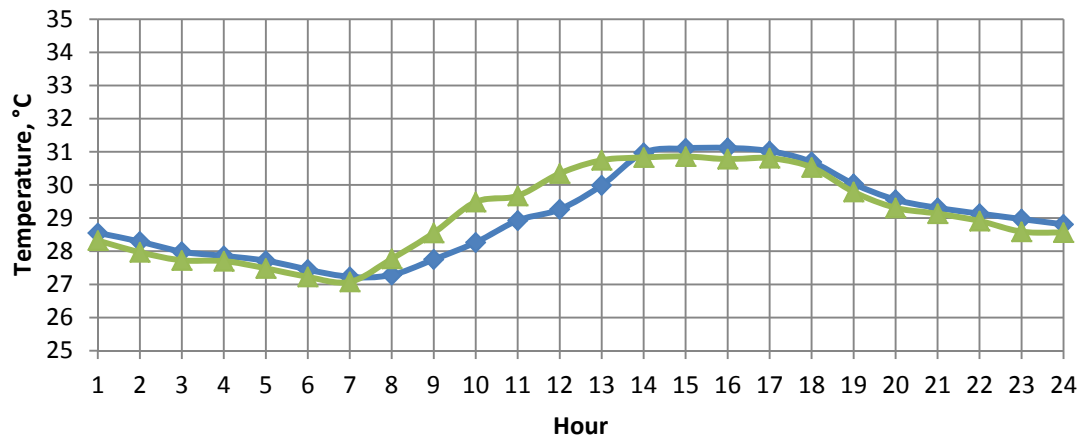
i) TP2
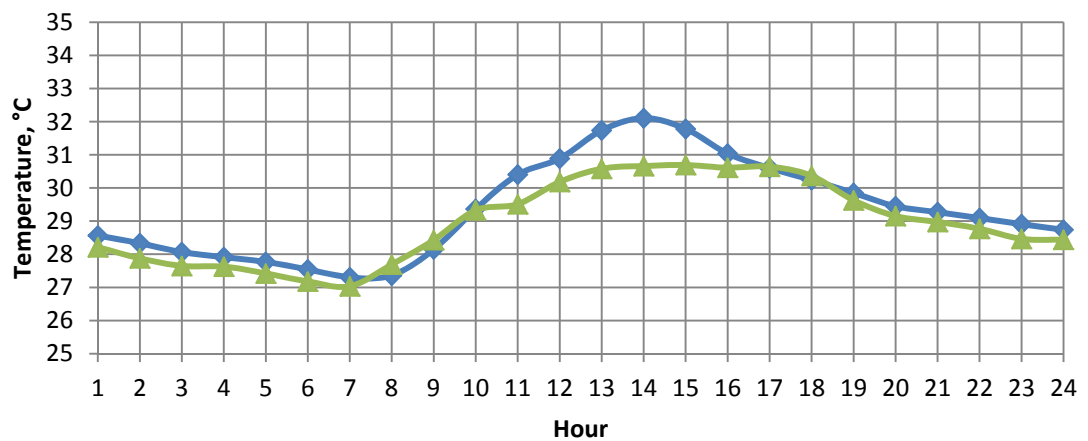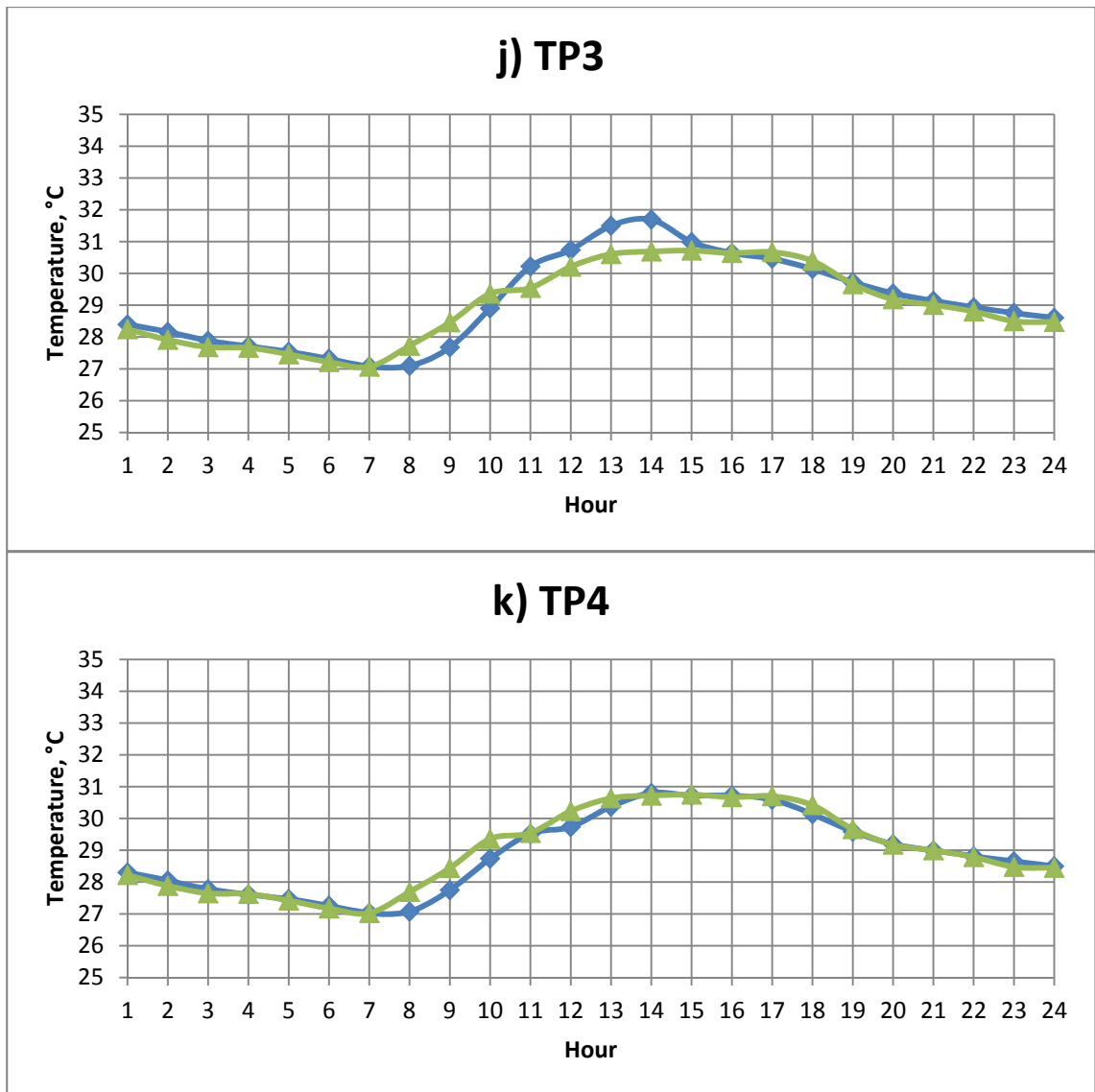
Figure 4.2a-k Measured and predicted 24 hour temperature profile for April

Agreement between measured and predicted temperature is further illustrated in figures 4.3 and 4.4. Figure 4.3 shows the scatter plot of predicted temperature against what was measured at every data point. It can be seen that the trend line ($y = 1.0011x$) for the predicted temperature closely follows that for measured temperature ($y = x$ connected with a series of red dots).Observation of the scatterplot also illustrates a linear relationship between measured and predicted temperature with a high R-squared value of 0.8861 Besides observation, the Pearson's chi-squared test was also used to assess the goodness of fit between measured and predicted data.

With 528 data points (Each point plotted in figures 4.1 a-k and 4.2 a-k = 1 data point), and a chi-square statistic of 3.18, it is obvious that the chi-square statistics do not exceed the lower tail critical value at 1% significance level (70.065 where degree of freedom = 100). This means that there is a less than 1% chance that any deviation from measured data is due to chance. Thus we do not reject the null hypothesis and conclude that there is no significant difference between the measured and modelled data.

Figure 4.4 is a box and whisker plot based on the average maximum, average minimum and the average 25th, 50th and 75th percentile of the measured and predicted temperature. The mean is illustrated by the blue line. From figure 4.4, it can be observed that both predicted and measured data have comparable ranges both between the box (25th and 75th percentile) and between the whiskers (minimum and maximum), with the measured data having a slightly higher temperature at maximum (0.2ºC) and the 75th percentile (0.25ºC). The other indicators (minimum, 25th percentile, median and mean) of the box and whisker plot also appears to be similar and not significantly different. Based on these observations along with error analysis described in the preceding paragraph, we can further affirm that the empirical model is able to calculate the typical 24 hour profile with sufficient accuracy.
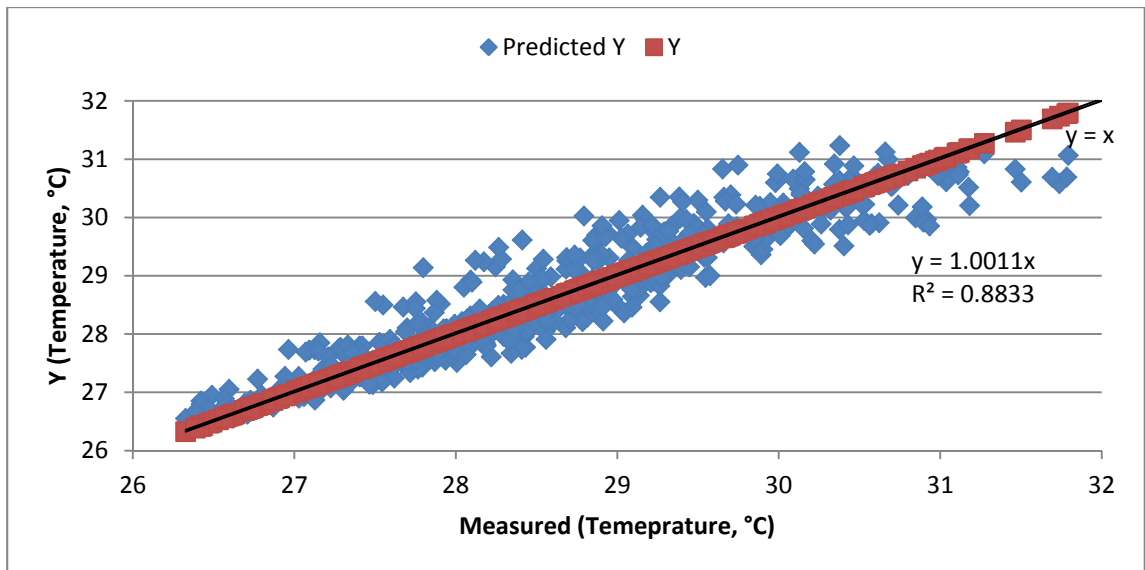
Figure 4.3 Blue points illustrating predicted temperature against measured. Red points illustrating line y = x or perfect prediction (months of March and April 2012)
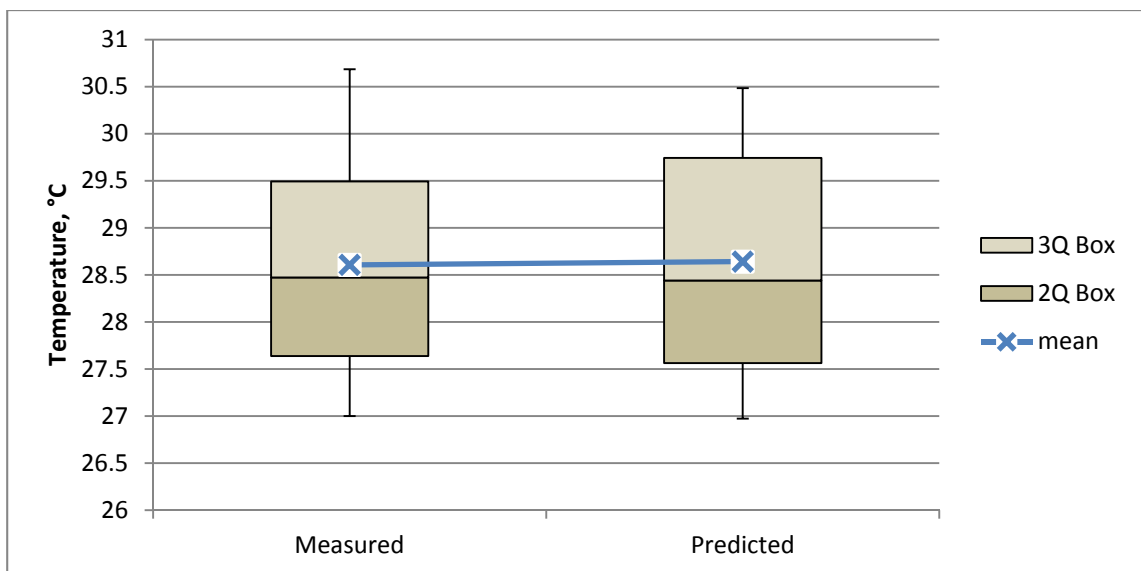
Figure 4.4 Box plot showing 3rd quartile, median and 2nd quartile with mean of measured and predicted data

4.2 Calculating change in conduction gains

Figures 4.5 to 4.7 show the scatter plot of the change in heat conducted through the wall, fenestration and roof against their respective U-value, area and sol-air temperature. Each of these parameters depends on the properties of the envelope as well as the external environment and has been evaluated as described in Chapter 3 above. The U-value was calculated based on the conductivity and thickness of the envelope components provided by the Building and Construction Authority (BCA) Singapore, and outside and inside surface coefficients as defined in Chapter 3. Based on each respective scatter plot, it can be seen that the possible increase in conduction gain is a linear function of the hypothesized independent variables. This is further affirmed by the high R-squared values (0.9895, 0.9513 and 0.9629) of each respective regression models. This fit was obtained with value of h_r that typically varies between 5 and 6 depending on the absorptance of the surface and the relevant environmental conditions.
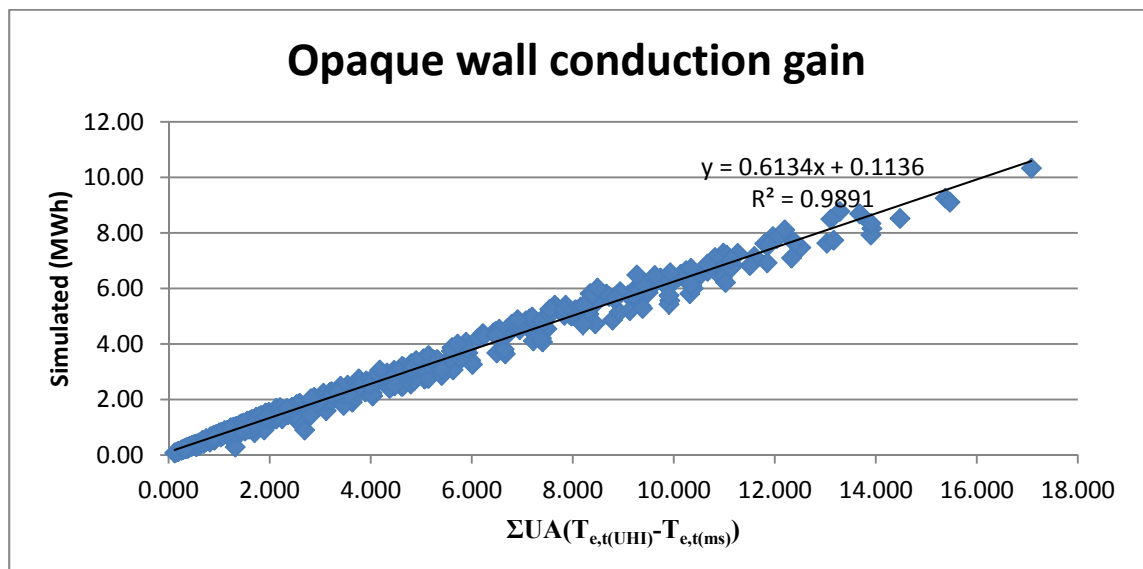
Figure 4.5 Simulated results against independent variables used to model conduction gain through opaque wall
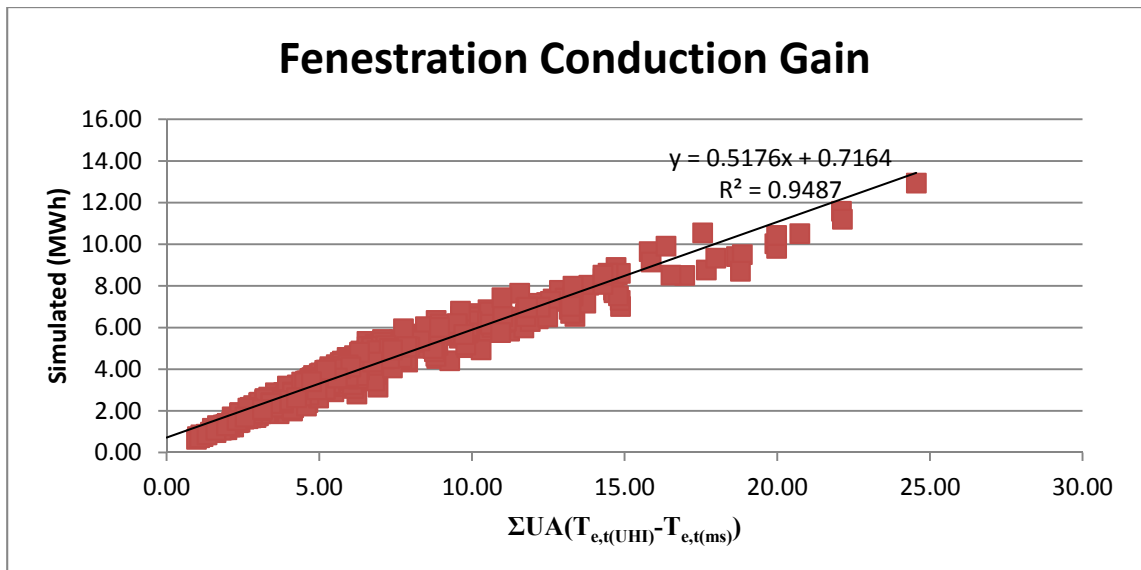
Figure 4.6 Simulated results against independent variables used to model conduction gain through fenestration
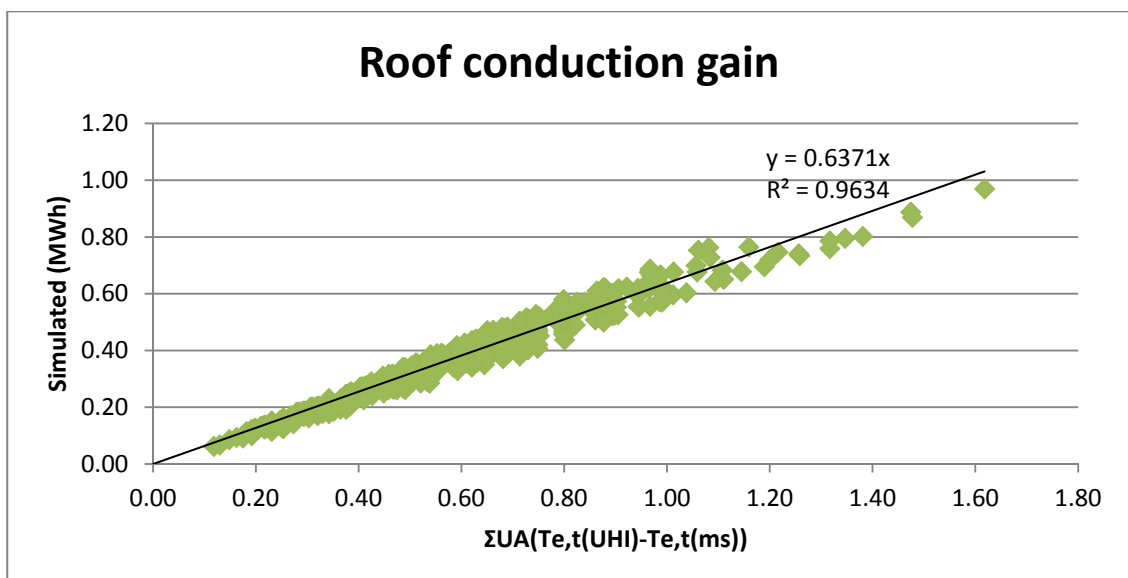
Figure 4.7 Simulated results against independent variables used to model conduction gain through roof

Using least squared estimation, the values of a and c can be extracted and subsequently used to calculate each of the respective gains. It is important to note that although there is a good fit between predicted and simulated results, the goodness of fit depends a lot on the temperature data through which the model uses as its input. Hence it is important that the urban morphology be accurately accounted for when calculating the 24 hour temperature profile for a particular locality.

4.3 Calculating solar heat gain through windows

Figures 4.8 and 4.9 shows the solar heat gain through windows calculated using equations 3.23 to 3.25 as compared to that obtained using simulation program IES-VE for the months of March to April and May respectively. From the two figures, it can be seen that the model used to calculate solar heat gain through glazing closely follows the results generated by the building energy simulation program. Observation of the scatterplot also illustrates a linear relationship between simulated and predicted temperature with a high R-squared value of 0.9913 and 0.9882 for the months of March and April, and May respectively.

The Pearson's chi-squared test was also used to assess the goodness of fit between measured and predicted data. With 286 data points and a chi-square statistic of 42, we can conclude that the chi-square statistics do not exceed the lower tail critical value at 1% significance level (70.065 where degree of freedom = 100). This means that there is a less than 1% chance that the calculated result would be significantly different from the simulated result. This means that there is a less than 1% chance that any deviation from simulated result is due to chance. Thus we do not reject the null hypothesis and conclude that there is no significant difference between the predicted and simulated result.
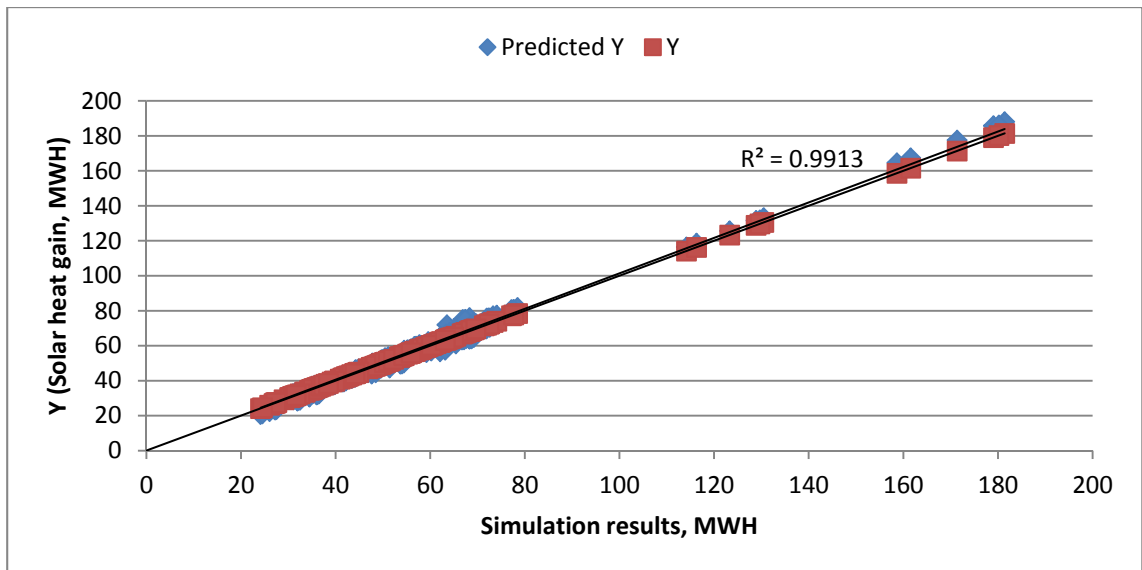
Figure 4.8 Simulated and predicted solar gain through glazing against simulation
results for March and April 2012
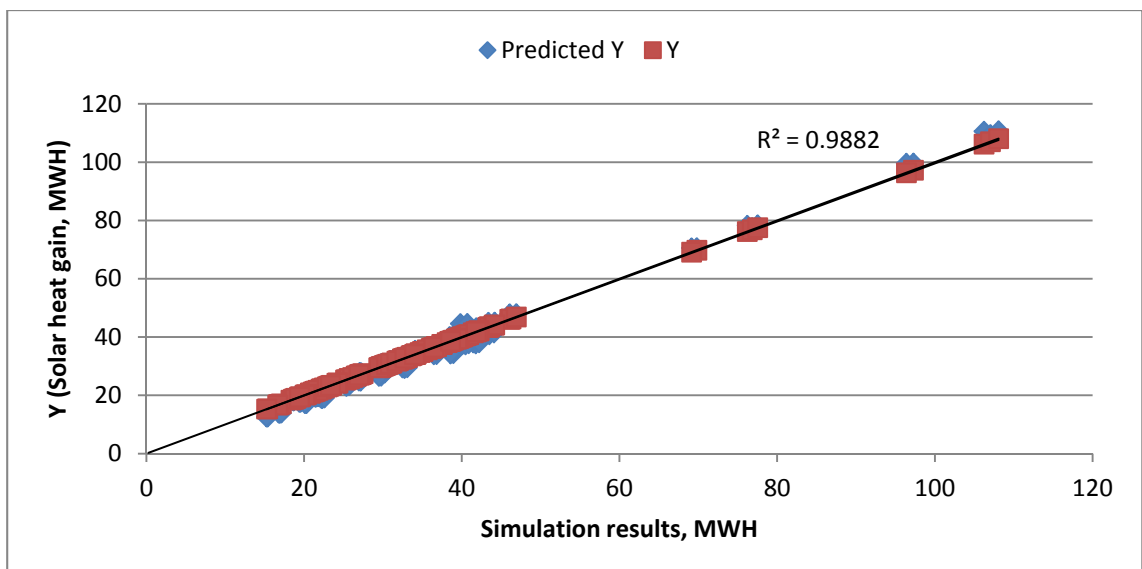
Figure 4.9 Simulated and predicted solar gain through glazing against simulation
results for May 2012

Chapter 5 Results and discussion

5.1 Application of tool

To provide an overview of an estate's environmental condition as well as the envelope performance of buildings within the estate, the average temperature map is integrated with calculations for conduction gains and solar heat gains. To illustrate, 8 buildings in the CBD area were selected (Figure 5.1). The 8 buildings were selected because of the completeness of data that were available for these buildings. Using detailed material and construction data on each of the building's façade provided by the Building and Construction Authority (BCA) of Singapore, window solar heat gains and the increase in conduction heat gains were calculated according to the methodology described in Chapter 3 above. Each surface of every building is calculated separately using exact window and wall areas provided by BCA with surface azimuths extracted from satellite data using GIS. Where data on wall and window areas are not available, they may be extracted using GIS. However, if this is to be used for regulating building envelope's performance, it is recommended that exact areas be used for precision. A 3-Dimensional model was also used for the calculation of the SkyEF (Figure 5.1). The calculated conduction gains and solar gains are then normalized by dividing by their respective envelope area.
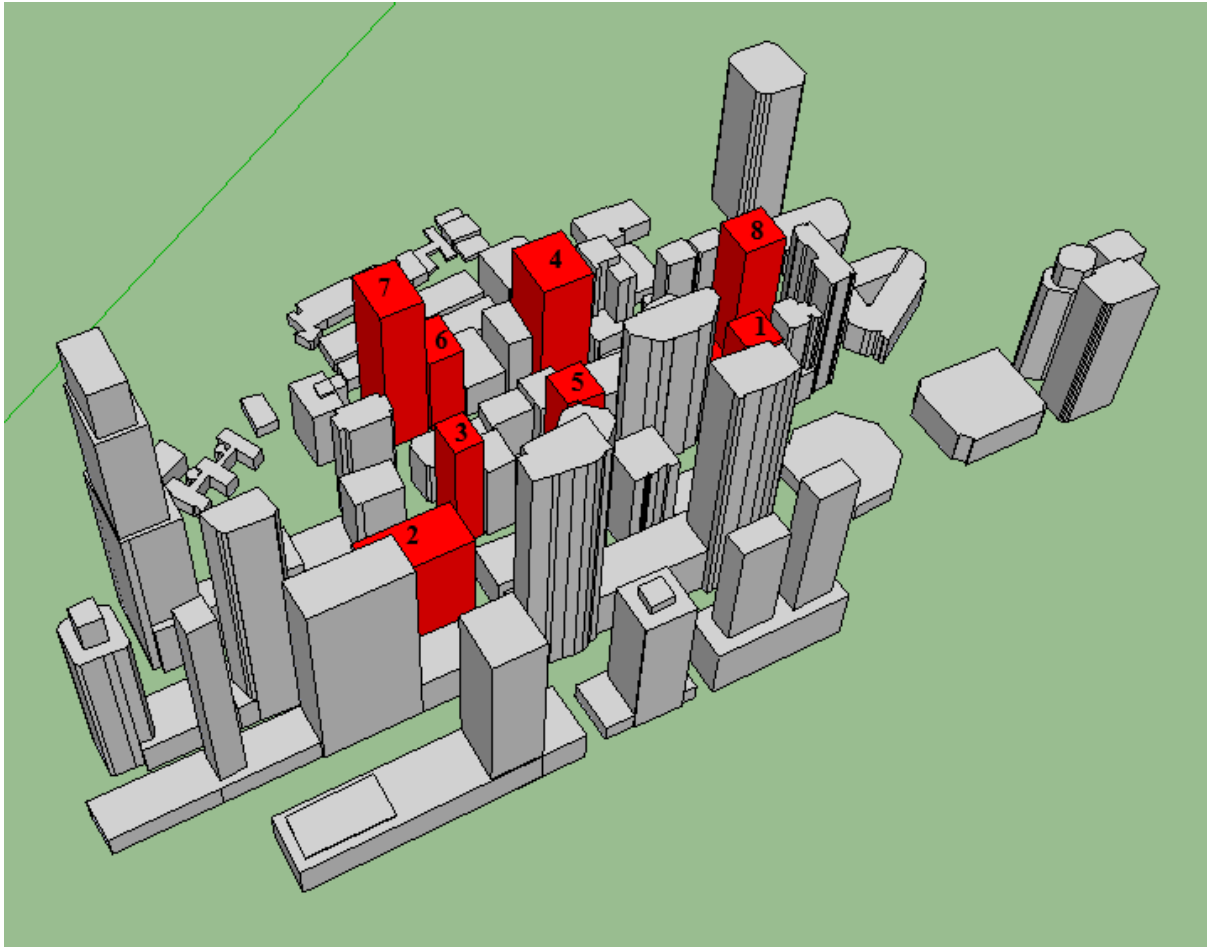
Figure 5.1 3-Dimensional model of buildings 1 to 8 and their surrounding built environment

Figures 5.2 shows the average temperature map integrated with the normalised conduction gain (Figure 5.2a) and normalised solar heat gain (Figure 5.2b). Using figure 5.2, buildings that have relatively poor envelope performance can be easily identified by their red colours. Since the scale used is a relative one, it also serves to benchmark buildings against each other.

According to figure 5.2a, buildings 5, 6 and 8 have relatively poorer performance amongst the 8 buildings when evaluated by the change in conduction gain brought about by UHI, with building 5 performing the worst. Aside from building 8 which has a higher average air temperature, the greater increase in conduction heat gain at buildings 5 and 6 is due to poor thermal resistance since the temperature map suggests that both buildings are not surrounded by significantly hotter spots when compared to

the surrounding of the other buildings. A look into the materials construction of buildings 5 and 6 reveals this observation to be true. The U-value (walls and windows) of building 5 and 6 averages at (2.71 W/m²K and 5.8 W/m²K) and (2.63 W/m²K and 1.6 W/m²K) respectively. This is relatively high given that the wall U-value of the other buildings generally falls below 1. In addition, the glazing used in building 5 is 8mm tinted single glaze, thus also contributing to its high conduction gain. It is also important to note that although building 8 is surrounded by higher air temperature due to its surrounding urban morphology, that is not the sole contributing factor. Its use of single glazing for windows (U-value 5.7 W/m²K) have also contributed to its relatively higher increase in conduction heat gain. However, it has acceptable wall U-value (average 0.67 W/m²K) and WWR (approximately 30 to 40 percent), which explains its better performance when compared to building 5.

From Figure 5.2b, it can be seen that building 5 also has the worst performance when evaluated by solar heat gain through glazing. This is despite being located at a densely built up area which provides significant shading from direct incoming solar radiation (Figure 5.1). Hence the high solar heat gain can be attributed to the type of glazing used which in this case is an 8mm tinted heat strengthened single glaze with a high SHGC of 0.83. Another observation is that although building 6 performs poorly when evaluated according to figure 5.2, the amount of solar heat gain through glazing is comparatively acceptable as seen by its yellow colour.

Hence it is important that buildings be evaluated by both the temperature maps, since poor performance in window solar heat gain does not signify the same for conduction heat gain. The seperation of conduction gains from solar heat gains also helps in identifying the areas of the building facades that requires the most attention.
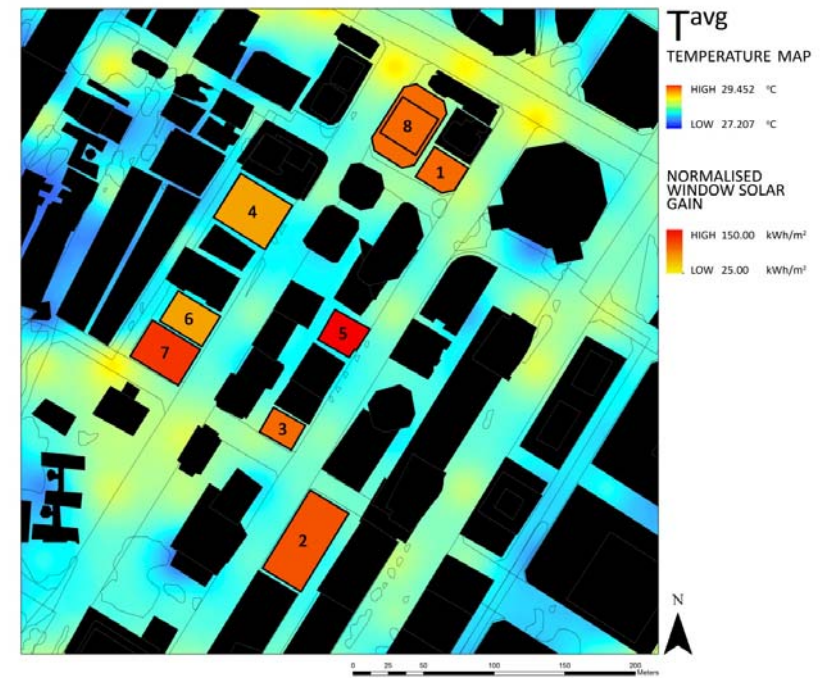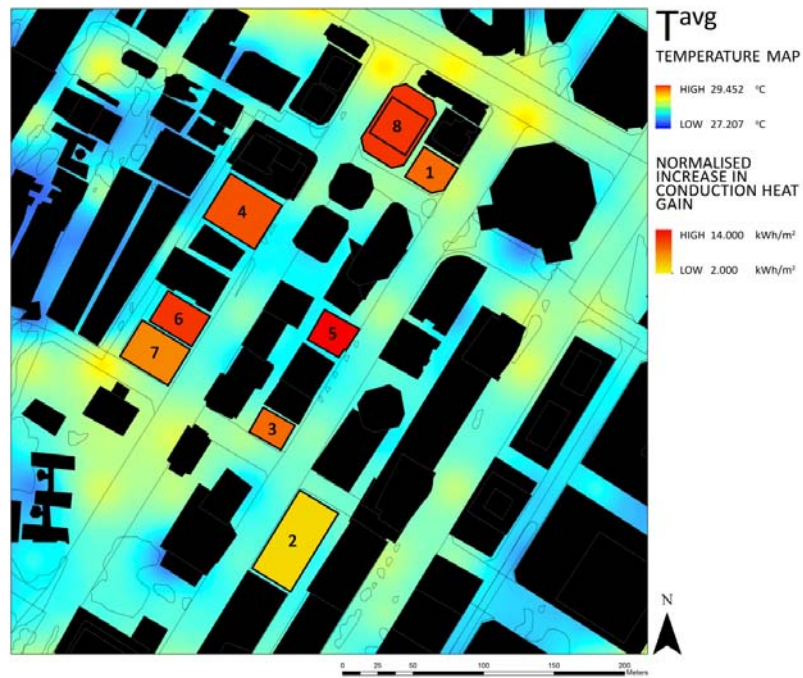
Figure 5.2 a) Normalized increase in conduction heat gain (left) and b) Normalized window solar heat gain (right)

Chapter 6 Conclusion

6.1 Summary

Urban development is imperative for economic growth and national development particularly in a small city-state such as Singapore without its own natural resources. With increasing urbanization and as population density increases, careful planning which incorporates the environment and any adverse impacts such as the urban heat island effect should be included. In particular, it would be beneficial if the evaluation of an urban environment can be extended to include its impact on buildings. This is because buildings account for 40% of global energy use with resulting carbon emission that are substantially more compared to the transport sector (WBCSD 2009). . In Singapore, 52% of energy consumed in a typical commercial building is for air conditioning (Lee, et al. 2004) and any heat island effect brought about by dense urban settings would effectively increase this percentage by increasing ambient air temperatures. Although some urban climatologists have developed building energy models which are integrated into urban canopy models (Kikegawa, et al. 2003; Salamanca, et al. 2009; Bueno, et al. 2011), the use of these numerical models and building energy simulation software can be time-consuming and costly particularly when done over a large area. Furthermore, building energy simulation models usually requires detailed building parameterizations and knowledge of HVAC configurations as input, which can be impractical for urban planners whose aim is to guide the physical development of the urban landscape in a sustainable manner. The objective of this study is therefore to develop a simple method that predicts the envelope performance of commercial office buildings in Singapore, taking into account the local urban microclimate. The aim is to develop a tool that makes use of readily

available data for use by urban planners and policy making, to guide and evaluate an estate's environmental condition while taking into account the building's façade performance and its surrounding urban parameters.

A total of 2 indicators of envelope performance were described in this study and they are the increase in conduction (Wall, Window and Roof) heat gain due to UHI effect (Equation 3.10) and the solar heat gain through windows taking into account the effect of shading by surrounding buildings and morphology (Equation 3.23). These indicators are then integrated with an average temperature map which accounts for the UHI effect, to provide a holistic overview of environmental conditions together with building performance. Such a tool may then be used by urban planners for planning purposes as well as by building authorities for regulating building performance. Both models for calculating the above mentioned heat gains are validated using building energy simulation programme IES-VE which uses the heat balance method for calculating each of the respective gains. Before conduction gains can be calculated, hourly air temperature data is required as input to the model and building simulation programme. Hence, to account for the impact of UHI effect on envelope performance, an empirical model (Equations 3.1 , 3.2 and 3.3) was developed to project a 24 hour profile of air temperature from maximum, minimum and average temperature (the output of STEVE tool). This empirical model has been validated using site measurements along Shenton Way and Tanjong Pagar which are located within the Central Business District of Singapore.

To illustrate the application of this tool, a total of 8 buildings in the Central Business District was selected and analysed using detailed material and construction of their facade provided by the Building and Construction Authority (BCA) of Singapore. Each surface of every building is calculated separately using exact window and wall

areas provided by BCA with surface azimuths extracted from satellite data using GIS. A 3-Dimensional model was also used for the calculation of the average SkyEF. The calculated conduction gains and solar gains are then normalized by dividing by their respective envelope area.

6.2 Limitations and future research

Although there is a good fit between what was predicted by the models described in Chapter 3 above and the results from building energy simulation programme IES-VE, these were based on a typical schedule and internal load of a commercial office building in Singapore. Hence, the calculated gains may not be reflective of buildings with schedule and internal loads that differs widely from typical Singapore offices.

The model uses calculations from STEVE tool as input for calculating the increases in conduction heat gain brought about by UHI effect. Hence it is important that the urban morphology be accurately accounted for when calculating the 24 hour temperature profile for a particular locality.

References

ASHRAE. *ASHRAE Handbook, 2009: Fundamentals.* Atlanta, GA: American Society of Heating Refrigerating and Air-Conditioning Engineers, 2009.

BFRC. "BFRC Guidance Note." http://www.ggf.org.uk/assets/windows-energy-ratings/Understanding-the-BFRC-Calculations.pdf (accessed 29 June 2012).

Born, M, and E Wolf. Born, M, and E Wolf, ed. *Principles of Optics: electromagnetic theory of propagation, interference and diffraction of light.* Pergamon, UK: Cambridge University Press, 1999.

Bueno, B, L Norford, G Pigeo, and R Britter. "Combining a Detailed Building Energy Model with a Physically-Based Urban Canopy Model." *Boundary-Layer Meteorol* (2011)

Chen, Liang, and Edward Ng. "Quantitative Urban Climate Mapping Based on a Geographical Database: A Simulation Approach Using Hong Kong as a Case Study." *International Journal of Applied Earth Observation and Geoinformation* 13 (2011): 586-94.

Chou, S.K, and W.L Chang. "Development of an Energy-Estimating Equation for Large Commercial Buildings." *International Journal of Energy research* 17 (1993): 759-73.

Chou, S.K, and Y.K Lee. "A Simplified Overall Thermal Transfer Value Equation for Building Envelopes." *Energy* 13, no. 8 (1988): 657-70.

Chua, K.J, and S.K Chou. "An ETTV-Based Approach to Improving the Energy Performance of Commercial Buildings." *Energy and Buildings* 42 (2010): 491-99.

Duffie, J. A, and W. A Beckman. *Solar Engineering of Thermal Processes.* New York: John Wiley and Sons, 2006.

El-Asfouri, A. S, M. F El-Refaie, and M. M Karawya. "Effect of Various Factors on the Shading Coefficient of Different Types of Glazing." *Building and Environment* 23, no. 1 (1988): 44-55.

Hawlader, M. N. A. "Diffuse, Global and Extra-Terrestrial Solar Radiation for Singapore." *International Journal of Ambient Energy* 5, no. 1 (1984): 31-38.

ICAO Standard Atmosphere. ICAO, ed. *Manual of the ICAO Standard Atmosphere Extended to 32 Kilometres (105,000 feet).* Montreal: International Civil Aviation Organization, 1964.

IES. "ApacheSim Calculation Methods (Virtual Environment 6.3)." http://www.iesve.com/support/userguides (accessed June 2012).

IES. "Constructions Databse User Guide: Virtual Environment 5.9." http://www.iesve.com/downloads/help/Thermal/ConstructionsDatabase.pdf (accessed 29 June 2012).

Jusuf, S. K, and N.H Wong. "Development of empirical models for an estate level air temperature prediction in Singapore." In *Second International Conference on Countermeasures to Urban Heat Island,* Berkley, California, 2009.

Jusuf, S. Kardinal, N.H Wong, E Hagen, R Anggoro, and H Yan. "The Influence of Land Use on the Urban Heat Island in Singapore." *Habitat International* 31 (2007): 232.242.

Katzschner, L, and J MÜlder. "Regional Climatic Mapping as a Tool for Sustainable Development." *J Environ Manage* 87 (2008): 262-67.

Kikegawa, Y, Y Genchi, H Yoshikado, and H Kondo. "Development of a Numerical Simulation System for Comprehensive Assessments of Urban Warming

Countermeasures Including their Impacts Upon the Urban Building's Energy-Demands." *Applied Energy* 76 (2003): 449-66.

Kinya, K, and K Koumura. "The Analysis of Greening Effects on the Urban Environment Using GIS." http://proceedings.esri.com/library/userconf/proc02/pap1159/p1159.htm (accessed June 2012).

Kruger, E, and B Givoni. "Outdoor Measurements and Temperature Comparisons of Seven Monitoring Stations: Preliminary Studies in Curitiba, Brazil." *Building and Environment* 42 (2007): 1685-98.

LBL. Windows and Daylighting Group, ed. *WINDOW 5.2: A PC program for analyzing window thermal performance for fenestration products. LBL-44789.* Berkeley: Lawrence Berkeley Laboratory, 2003.

Lee, S.E, W Schafer, and H.S Majid. *Energy Performance Assessment and Classification of Commercial Buildings in Singapore (Report No. NUS Project No: R-296-0056-490/R-296-0056-592).* Singapore: NUS, CTBP, 2004.

Liu, B. Y. H, and R. C Jordan. "The Interrelationship and Characteristic Distribution of Direct, Diffuse and Total Solar Radiation." *Solar Energy* 4 (1960): 1-19.

Oke, T. R. "Canyon Geometry and the Nocturnal Urban Heat Island: Comparison of Scale Model and Field Observations." *Journal of Climatology* 5 (1981): 237-54.

Oke, T.R. "The energetic basis of the Urban Heat Island." *Quart. J. R. Met. Soc.* 108 (1982): 1-24.

Ong, B. L. "Green plot ratio: an ecological measure for architecture and urban planning." *Landscape and Urban Planning* 63 (2003): 197-211.

Ruth, D. W, and R. E Chant. "The Relationship of Diffuse Radiation to Total Radiation in Canada." *Solar Energy* 18, no. 2 (1976): 153-54.

Salamanca, F, A Krpo, A Martilli, and A Clappier. "A New Building Energy Model Coupled with an Urban Canopy Parmeterization for Urban Climate Simulations-Part 1. Formulation, Verification, and Sensitivity Analysis of the Model." *Theor Appl Climatol* 99 (2009): 331-44.

Santamouris, M, D.N Asimakopoulos, V.D Assimakopoulos, N Chrisomallidou, N Klitsikas, D Mangold, and A Tsangrassoulis. Santamouris, M, ed. *Energy and Climate in the Urban Built Environment.* London, UK: James & James Ltd, 2001.

SS 531. *Singapore standard SS 531: Code of Practice for Lighting of Work Places Part 1: Indoor.* Singapore: Spring Singapore, 2006.

SS 553. *Singapore Standard SS 553: Code of Practice for Air-Conditioning and Mechanical Ventilation in Buildings.* Singapore: Spring Singapore, 2009.

Turiel, I, R Boschen, M Seedall, and M Levine. "Simplified Energy Analysis Methodology for Commercial Buildings." *Energy and Buildings* 6 (1984): 67-83.

U.S. Standard Atmosphere. *U.S. Standard Atmosphere.* Washington, D.C: U.S. Government Printing Office, 1976.

UIUC, and LBNL. "EnergyPlus Engineering Reference: The reference to EnergyPlus Calculations." http://apps1.eere.energy.gov/buildings/energyplus/pdfs/engineeringreference.pdf (accessed May 2012).

WBCSD. "Energy Efficiency in Buildings." http://globealliance.org/Libraries/Resources/WBCSD_Energy_Efficiency_in_Buildings.sflb.ashx (accessed November 2011).

Wong, N. H, and S. K Jusuf. "An assessment method for existing greenery conditions in a university campus." *Architectural Science Review* 51, no. 3 (2008): 116-26.

Wong, N. H, and S. K Jusuf. "GIS-based greenery evaluation on campus master plan." *Landscape and Urban Planning* 84 (2008): 166-82.

Wong, N.H, D.K.W Cheong, H Yan, J Soh, C.L Ong, and A Sia. "The Effects of Rooftop Garden on Energy Consumption of a Commercial Building in Singapore." *Energy and Buildings* 35 (2003): 353-64.

Zhang, J, C. K Heng, L. C Malone-Lee, D. J. C Hii, P Janssen, K. S Leung, and B. K Tan. "Evaluating Environmental Implications of Density: A Comparative Case Study on the Relationship between Density, Urban Block Typology and Sky Exposure." *Automation in Construction* 22 (2012): 90-101.

Appendix A

Table A.1 27 different envelope combination based on survey of buildings around central business district in Singapore

Wall Constrution (outside -inside)	Window construction (outside- inside)	Roof construction (outside- inside)	WWR
5mm alum panel, 75mm insulation, 100mm air gap, 20mm plaster board, U-value = 0.386	8mm anti-sun float bronze, 12mm airspace, 6mm clear float, U-value = 2.930, SC = 0.37	12.5mm roof gravel, 9.5mm built up roofing, 50mm polystyrene insulation, 150mm concrete slab, 102mm air layer, 13mm acoustic tile, U-value = 0.637	0.40
478mm glass sheet, 130mm air gap, 75mm glass wool, 18mm plaster gypsum, U-value = 0.331	8mm grey tinted low-E heat strengthened, 12mm airspace, 8mm clear heat strengthened, U-value= 1.412, SC = 0.29	12mm tiles, 25mm screed, 50mm vermiculite, 50mm screed, 300mm concrete, U-value = 0.771	0.37
30mm Aluminium cladding, 50mm air gap, 350mm concrete wall, 20mm plaster-cement/sand, U-value = 1.817	6mm clear float, 12mm airspace, 6mm clear float, U-value= 3.005, SC= 0.31	75mm Precast slab, 25mm polystyrene insulation, 150mm concrete, U-value = 0.862	0.52
6mm Single glaze glass, 110mm air gap, 1.2mm Aluminium Back panel, 50mm Rockwool, U-value= 0.567	6mm/ 12mm air gap/ 6mm double glaze glass, U-value = 1.636, SC= 0.27	12.5mm roof gravel, 9.5mm built up roofing, 50mm polystyrene insulation, 150mm concrete slab, 102mm air layer, 13mm acoustic tile, U-value = 0.637	0.57
6mm Single Glaze glass, 70mm air gap, 1.2mm Aluminium Back panel, 50mm Rockwool, 200mm air gap, 100mm Light weight concrete, 200mm air gap, 50mm rockwool, 12mm gypsum board, 3mm timber panelling, U-value= 0.145	6mm/ 12mm air gap/10mm double glaze glass, U-value = 1.636, SC= 0.38	12.5mm roof gravel, 9.5mm built up roofing, 50mm polystyrene insulation, 150mm concrete slab, 102mm air layer, 13mm acoustic tile, U-value = 0.637	0.57
8mm glass, 122mm air gap, 1.5mm Aluminium backpan, 50mm rockwool insulation with aluminium foil, U-value = 0.390	VRE 19-54 Glass (all vision) 6mm crystal gray, 12mm air gap, 6mm clear, U-value =1.50, SC= 0.3	50mm cement plaster, 50mm polystyrene, 50mm cement plaster, 200mm RC, U-value = 0.541	0.58
1.2mm Galvanised Steel Sheet, 50mm Rockwool, U-value = 0.626	6mm tinted glass, 12mm air gap, 6mm tinted glass, U-value= 1.683, SC = 0.33	12.5mm roof gravel, 9.5mm built up roofing, 50mm polystyrene insulation, 150mm concrete slab, 102mm air layer, 13mm acoustic tile, U-value = 0.637	0.53
20mm plaster, 230mm Brickwall, 20mm plaster, U-value= 1.887	6mm/12mm air gap/6mm double glazing, U-value= 1.683, SC = 0.33	50mm cement/sand panel roofing, 50mm polytyrene insulation, 25mm cement/sand screed, 130mm RC slab, U-value = 0.547	0.40
6mm glass sheet, 20mm air gap, 20mm plaster, 100mm Brickwall, 20mm plaster, U-value= 2.060	6mm/12mm air gap/6mm double glazing, U-value= 1.683, SC = 0.33	50mm cement/sand panel roofing, 50mm polytyrene insulation, 25mm cement/sand screed, 130mm	0.40

		RC slab, U-value = 0.547	
12mm plaster, 200mm Brickwall, 12mm plaster, U-value = 2.161	13mm dark blue laminated, U-value= 5.487, SC= 0.9	12.5mm roof gravel, 9.5mm built up roofing, 50mm polystyrene insulation, 150mm concrete slab, 102mm air layer, 13mm acoustic tile, U-value = 0.637	0.59
20mm plaster, 200mm Brickwall, 20mm plaster, U-value= 2.618	8mm tinted heat strengthened glass, U-value= 5.632, SC=0.99	12.5mm roof gravel, 9.5mm built up roofing, 50mm polystyrene insulation, 150mm concrete slab, 102mm air layer, 13mm acoustic tile, U-value = 0.637	0.38
20mm plaster, 150mm Brickwall, 20mm plaster, U-value= 2.667	6mm/ 12mm air gap/ 6mm Bronze tinted low-E, U-value= 1.585, SC= 0.33	12.5mm roof gravel, 9.5mm built up roofing, 50mm polystyrene insulation, 150mm concrete slab, 102mm air layer, 13mm acoustic tile, U-value = 0.637	0.39
4mm Alucobond, 25mm Rockwool insulation, 100mm space gap, 25mm Aluminium, 40mm space gap, 25mm Aluminium, 28mm glass, 25mm Aluminium, U-value = 0.517	28mm Low E double glaze, U-value= 1.585, SC = 0.34	50mm cement/sand screed, 50mm thermal insulation, waterproof membrane, 25mm cement/sand screed, 200mm concrete slab, 12mm cement skim coat, U-value = 0.501	0.65
150mm Spandral glass, 1mm Aluminium, air gap, 1mm aluminium, U-value=1.36	Low-E double glaze, U-value= 1.585, SC= 0.32	12.5mm roof gravel, 9.5mm built up roofing, 50mm polystyrene insulation, 150mm concrete slab, 102mm air layer, 13mm acoustic tile, U-value = 0.637	0.59
30mm Granite, 100mm air gap, 50mm mineral wool, 3mm Aluminium lining, U-value= 0.618	6mm/12mm air gap/6mm double glazing, U-value= 1.683, SC = 0.27	50mm cement panel, 50mm polystyrene insulation, 200mm RC slab, U-value = 0.5149	0.54
30mm Granite, 70mm air space, 500mm concrete, U-value= 1.4685	8mm/8mm air gap/ 8mm double glazzing, U-value= 2.02, SC= 0.42	75mm light weight panel roofing, 50mm polystyrene insulation, 50mm cement/sand screed, 150mm RC slab, U-value = 0.528	0.56
20mm cement plaster, 200mm RC wall, 20mm cement plaster, U-value= 2.606	8mm clear glass/ 12mm air gap/ 6mm clear glass, U-value = 1.585, SC= 0.28	12.5mm roof gravel, 9.5mm built up roofing, 50mm polystyrene insulation, 150mm concrete slab, 102mm air layer, 13mm acoustic tile, U-value = 0.637	0.32
19mm plaster, 115mm RC wall, 19mm plaster, U-value= 3.504	6mm tinted double glazed glass, U-value= 2.930, SC= 0.26	20mm waterproofing cement screeding, 75mm lightweight concrete, 120mm RC slab, U-value = 0.326	0.35

3mm Aluminium cladding, 25mm Fiberglass, U-value= 1.131	8mm Tinted glass, U-value 5.632, SC= 0.42	50mm cement/sand panel, 1mm roofing felt, 25mm polystyrene insulation, 3mm bituminous membrane, 25mm cement/sand screed, 150mm RC slab, U-value = 0.883	0.34
20mm plaster, 200mm RC wall, 20mm plaster, U-value= 2.606	6mm/ 12mm air gap/ 6mm double glaze glass, U-value = 3.233, SC = 0.38	50mm cement/sand screed, 50mm polystyrene insulation, 200mm RC slab, U-value = 0.546	0.30
6mm spandrel, 80mm air gap, 36mm insulation, 12mm gypsum board, U-value 0.525	6mm tinted single glaze, U-value = 5.693, SC = 0.48	2.5mm roof gravel, 9.5mm built up roofing, 50mm polystyrene insulation, 150mm concrete slab, 102mm air layer, 13mm acoustic tile, U-value = 0.637	0.38
30mm granite, 45mm air gap, 125mm RC wall, 50mm wood wool slab, 12mm gypsum board, U-value = 1.271	6mm/ 12mm air gap/ 6mm double glaze glass, U-value = 3.233, SC = 0.42	50mm cement/sand panel, 50mm polystyrne board, 25mm cement/sand screed, 150mm RC slab, U-value = 0.543	0.48
30mm Granite, 65mm air gap,100mm RC wall, 10mm cement plaster, U-value= 2.363	6mm reflective glass/ 12mm air gap/ 6mm clear glass, U-value = 3.233, SC = 0.26	50mm concrete panel, 50mm woodwool insulation, 25mm cement screed, 150mm RC slab, U-value = 1.176	0.26
30mm Granite, 50mm Air gap, 600mm concrete, U-value = 1.355	8mm/8mm air gap/ 8mm double glazing, U-value= 2.889, SC= 0.43	25mm cement/sand plaster, 25mm Polyurethane insulation foam, 150mm lightweight concrete, 20mm cement/sand plaster, U-value = 0.621	0.41
32mm Granite, 118mm air gap, 200mm brickwall, U-value = 1.945	6mm/ 12mm air gap/ 6mm tinted double glaze glass, U-value = 3.233, SC = 0.28	75mm precast concrete panel, 50mm polyurethane insulation foam, 30mm cement/sand screed, 125mm RC slab, U-value = 0.408	0.34
3mm aluminium cladding, 170mm air gap, 12mm gypsum plaster board, 50mm fibre glass insulation, 12mm gypsum plaster board, U-value = 0.698	6mm/12mm air gap/6mm reflective double glazing, U-value= 3.233, SC = 0.30	25mm waterproof cement, 3mm motar plas std water, 75mm lightweight concrete screed, 120mm RC slab, U-value = 0.842	0.45
3mm aluminium panel, 50mm air gap, 50mm rock wool, 200mm air gap, 125mm brickwall, U-value= 0.485	single glaze, 6.38mm thk (emilam RB-20), U-value = 5.681, SC = 0.45	2.5mm roof gravel, 9.5mm built up roofing, 50mm polystyrene insulation, 150mm concrete slab, 102mm air layer, 13mm acoustic tile, U-value = 0.637	0.41

Publications

Chong, Z. M. A, Wong N H. (2011). A generalized methodology for determining the increase in total heat gain through building envelopes due to climate change. Paper presented at ISUF 2011 conference. Montréal, Quebec, Canada.

Chong. Z. M. A, Ignatius M, Wong N H, Jusuf S K. (2012). The effect of urban heat island on heat gain increase. To be presented at The 8th International Conference on Urban Climates (ICUC8). Dublin, Ireland.